SEISMIC RETROFIT OF CONCRETE BLOCK WALL INTERSECTIONS

STRENGTHENING OF CONCRETE BLOCK WALL INTERSECTIONS USING GFRP LAMINATES

By

STEVE GEORGE, B.ENG.

A Report

Submitted to the School of Graduate Studies

in Partial Fulfilment of the Requirements

for the Degree

Master of Engineering (M.Eng.)

McMaster University

MASTER OF ENGINEERING (2008) McMaster University
(Civil Engineering) Hamilton, Ontario

TITLE: Strengthening of Concrete Block Wall Intersections using GFRP Laminates

AUTHOR: Steve George, B.Eng. (McMaster University, 2005)

SUPERVISOR: Dr. Wael W. El-Dakhakhni (McMaster University)

NUMBER OF PAGES: vi, 77

ACKNOWLEDGEMENTS

I wish to convey my gratitude to Dr. Wael W. El-Dakhakhni for his guidance, encouragement and insight. This project could not have been successfully completed without his advice during the experimental phase and the compilation of this report. I would also like to thank Dr.A. Ghani Razaqpur for being the second reader of this report and providing valuable advice.

The work presented herein was part of ongoing masonry research in McMaster University Center for Effective Design of Structures (CEDS). Funding was provided through the Ontario research and Development Challenge Fund (ORDCF). This research area fall under the CEDS Focus Area 1: Masonry Structures, CEDS Focus Area 2: Earthquake Engineering, CEDS Focus Area 3: Investigation and Remediation of Structures, and CEDS Focus Area 4: Enhanced Use of New and Under-Utilized Materials.

Donation of mason's time by the Canada Masonry Design Centre (CMDC), FRP materials by Fyfe Co., San Diego, California and Truss type Joint reinforcement by BLOK-LOK Ltd., Toronto, Ontario are gratefully recognized. Special thanks to McMaster University technicians David Perrett, Kent Wheeler and Rhys Westmoreland.

I want to thank all my professors and classmates who have been instrumental in shaping my academic career as an undergraduate and graduate student. Last, but not least, I must thank my parents and my sister for always supporting me and always pushing me to be a better professional and human being. I would not have been able to come this far without their love and guidance.

TABLE OF CONTENTS

LIST OF FIGURES

LIST OF TABLES

ABSTRACT

An experimental investigation was conducted to analyze the effectiveness of repairing and retrofitting the intersections of flanged concrete block shear walls using surface-bonded fiber-reinforced polymer (FRP) laminates for seismic load applications. A total of 18 specially designed flange-web intersecting wall assemblages were tested using 5 different schemes. Tests included wall intersections reinforced with unidirectional FRP with the fibers oriented perpendicular to loading direction (90^o), parallel to loading direction (0^o) and bi-directional ($90^o/0^o$), $(90^o/0^o)^2$ and ($45^o/135^o$) to applied load direction. The behaviour of each wall specimen is discussed with respect to its failure mode, strength and deformation characteristics. Results showed that the laminates significantly increased the shear strength of concrete block shear walls junction. In addition, the fiber orientation influenced the failure mode, strength and stiffness. Moreover, depending on the fiber orientation, a significant enhancement to the post-peak load energy absorption capacity of the web-flange intersection can occur. The improved post-peak behaviour addressed the benefits of retrofitting concrete block wall intersections for seismic load applications. The FRP-retrofitted specimens were capable of reaching between 90% to 390% increase in strength compared to the unretrofitted specimen constructed with traditional steel joint reinforcement.

INTRODUCTION

Medium height buildings with masonry shear walls are common in urban centers. Typically the limited ductility of these buildings results in relatively large lateral seismic design loads. Therefore, T, I-, C-, Z-, L-, and W-shaped wall cross sections (see Fig. 1) are often required to provide sufficient flexural strength [Paulay and Priestley (1992)]. The addition of flanges to wall cross section area is highly effective in increasing the resistance to bending but the resulting increase in the lateral shear force due to the increased stiffness can create a problem. Adding flanges does not significantly improve resistance to these shear forces. In fact, a specific concern exists about the localized shear effect resulting from the sudden change of section at the flange-web intersection. Moreover, the methods used to connect the web and the flanges may also have an impact on the shear capacity of this joint and the structural integrity of the flanged wall. If the connection between the web and the flange is not properly designed to withstand the shear stresses induced by the expected lateral design forces, then a significant portion of the shear walls' stiffness and strength will be lost.

Clause 1.9.4 of ACI530-05/ASCE5-05/TMS402-05 (MSJC, 2005) addresses the design of intersecting walls and states that, for the transfer of shear between walls, wall intersections or the connection should conform to one of the certain requirements. However, no recommendations are provided in the MSJC (2005) Code on how to calculate the actual shear transfer requirements at the flange-web intersection.

Structurally connecting intersecting (orthogonal) block walls and strengthening the web-flange intersection in existing masonry buildings is being recognized as a cost-effective technique to increase the strength of masonry buildings to conform to new seismic code provisions (Drysdale et al., 2008). Flanged walls are self-bracing against out-of-plane deformations which also minimizes the slenderness effects (Drysdale et al. 2005). However, if the connections between the flanges and the webs are not designed and detailed properly, the composite action of the web and flanges may not be realized because of the reduced capabilities of the intersection to transfer interfacial shear across the flange-web interface [Fig. 2]. This also minimizes the effectiveness of the flanges in providing bending resistance and lateral stability.

Current practice in North America utilizes horizontal truss-type joint reinforcement (see Fig. 3) continuous across the intersection to provide the connection between intersecting walls. This paper presents the experimental results of a research program aiming at developing a cost-effective technique for retrofitting intersecting concrete block walls in masonry buildings. Retrofitting may be required due to changes in design loads that may result from the lack of accurate design data at the time the building was constructed, alteration in building occupancy or renovations, or adoption of more stringent seismic code provisions.

Conventional retrofit techniques associated with the addition of framing members or new walls are labor intensive, consume substantial valuable space and are intrusive. These factors cause buildings to loose their functionality during retrofitting and cause significant economic impact to building users and owners. In the past two decades, extensive research efforts focused on evaluating the application of FRPs in strengthening masonry walls subjected to out-of-plane or in-plane loads (Triantafillou 1998; Velazquez-Dimas and Ehsani 2000; Albert et al. 2001; Hamilton and Dolan 2001; Hamoush et al. 2001; Kuzik et al. 2003; Tan and Patoary 2004; Ehsani et al. 1997; Hamid et al. 2005). However, no work was conducted on strengthening the connection between intersecting masonry walls or to create this connection when needed. Unlike traditional FRP laminate retrofit of masonry walls against in-plane and out-of-plane loading, FRP connection of intersecting walls is challenging because of the geometry of the connection. The sharp change in FRP orientation creates a need to examine failure modes and deformation characteristics at the flange-web intersections. Therefore, an experimental investigation was conducted to assess and evaluate the strength of the FRP/wall system in transferring the interfacial shear from the web to the flanges and hence enhance or act as a replacement of conventional steel joint reinforcement.

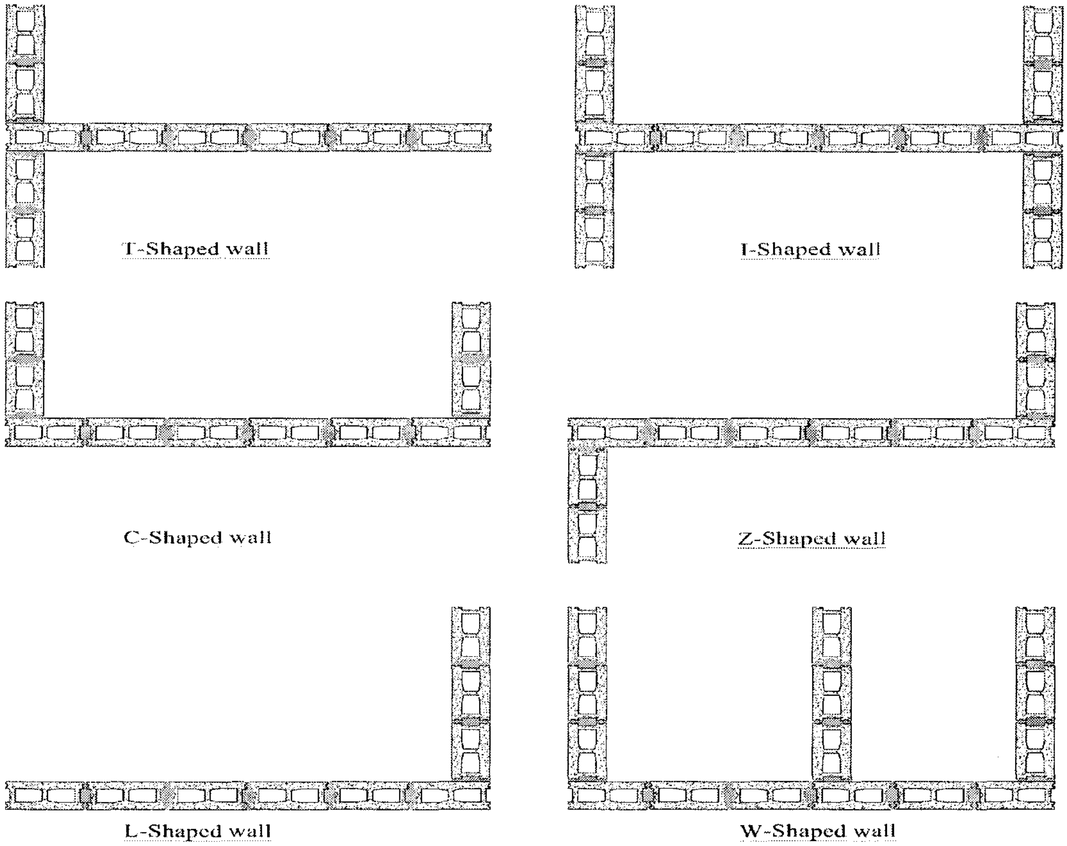

Figure 1: Different configuration of intersecting masonry shear walls

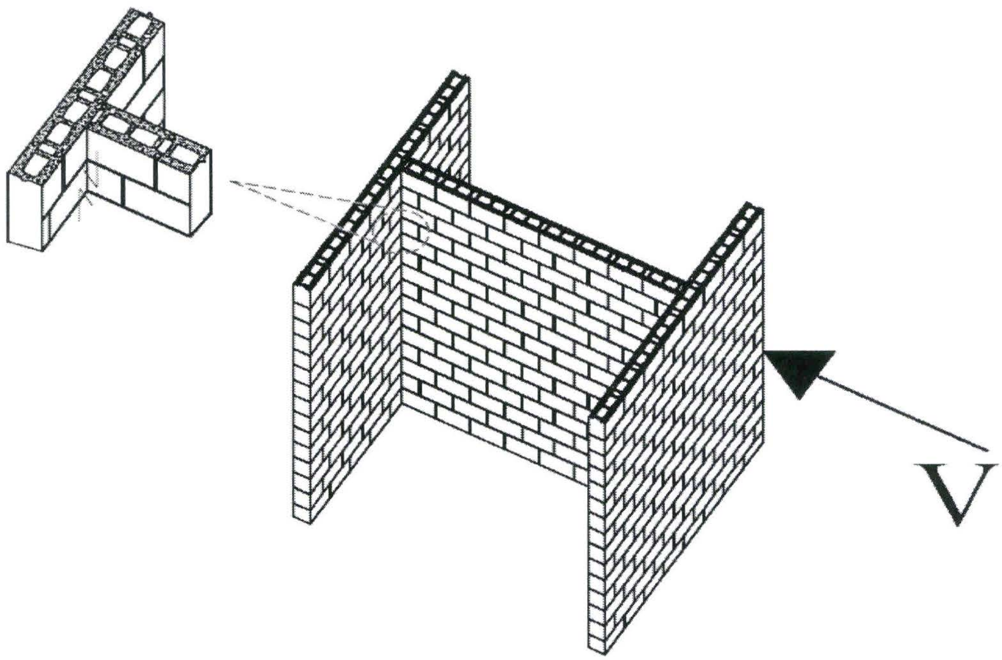

Figure 2: Interfacial Shear at intersecting Shear Walls

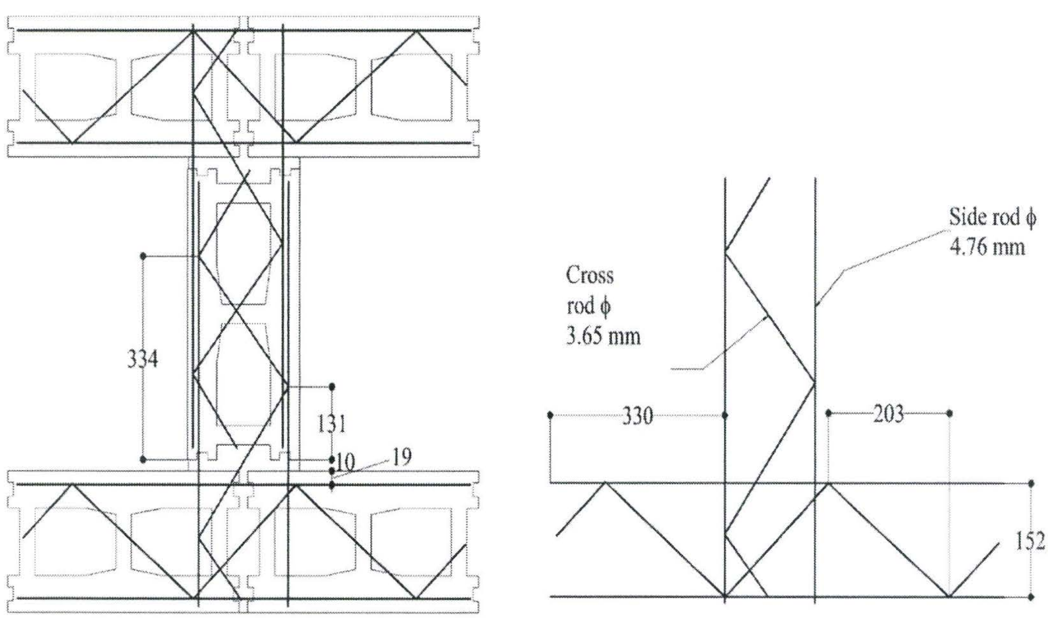

Dimensions in mm

Figure 3: Horizontal truss-type joint reinforcement

DEVELOPMENT OF TEST METHOD

The selection of an appropriate specimen configuration was based on work of Drysdale et al., 2008. The following sections will summarize and discuss the choice of the most appropriate specimen configuration. In their study, Drysdale et al., 2008 conducted an exploratory investigation to study the behavior of flanged concrete block masonry walls. Seven prototype specimens were tested prior to finalizing an appropriate specimen that was able to simulate the interfacial shear transfer occurring at the flange-web interface regions of intersecting shear walls. The objective of the research was to produce the desired failure mode, simulate field construction, ensure simple construction and testing, and to create a statically determinate specimen, to avoid difficulties in interpreting the test results.

Lessons learned through the experimental work performed on prototype specimens led to the selection of the configuration of the final specimens [Fig. 4]. To assist with the interpretation of results only one Truss-Type Joint Reinforcement (TTJR) was used per intersection. To facilitate measurement and development of post-cracking deformation, a 200mm gap was left below the web blocks. To minimize the bending stresses on the flange-web intersections, loading and support lines were kept as close as possible, as shown in Fig. 4, to minimize eccentricities and additional bending stresses across the interface.

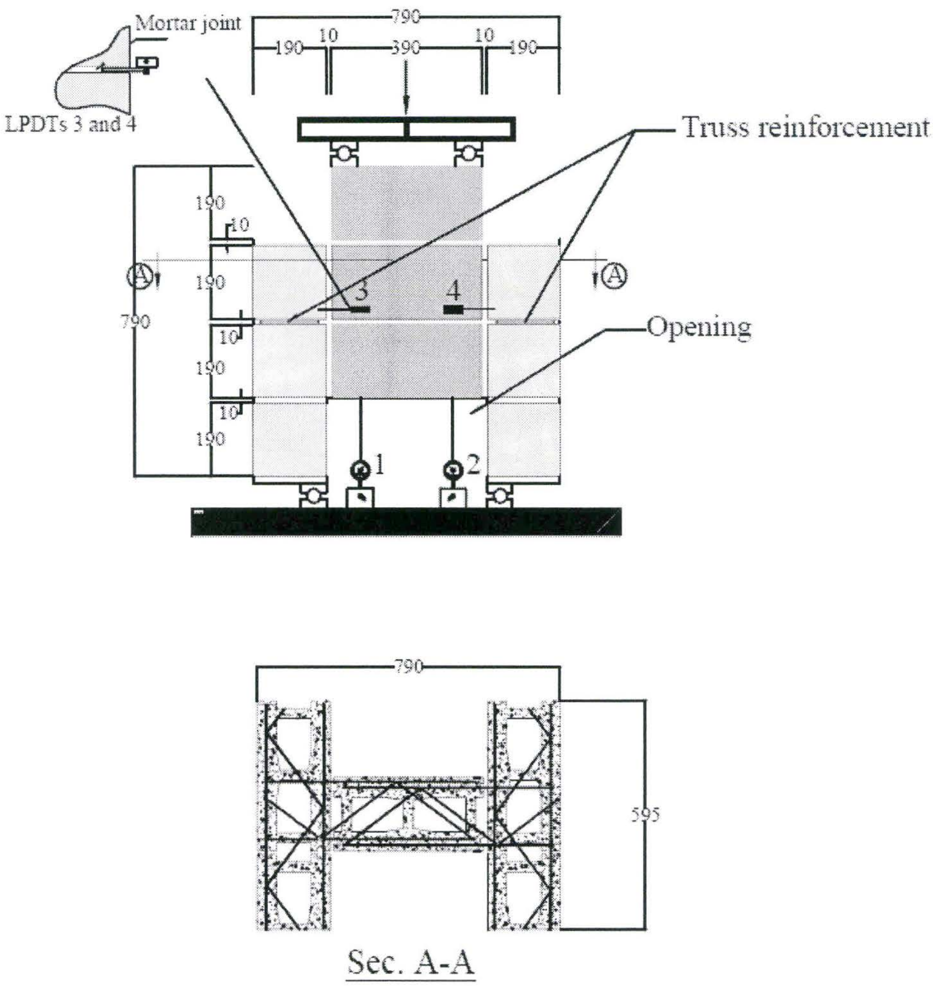

Figure 4: Assemblage size and configuration

EXPERIMENTAL PROGRAM

The primary objective of the present experimental study is to investigate the effects of different FRP retrofit schemes on the failure mode, strength and deformation characteristics of the retrofitted intersecting block walls. The following retrofitted specimens were tested with three repeat specimens in each case:

1. Series **R90°** with unidirectional fiber oriented perpendicular (90°) to load direction;
2. Series **R0°** with unidirectional fiber oriented parallel (0°) to load direction;
3. Series **R90°/0°** with bi-directional fiber oriented at (90°/0°) to load direction;
4. Series **R(90°/0°)^2** with two layers of bi-directional fibers oriented at (90°/0°) to load direction; and,
5. Series **R45°/135°** with bi-directional fiber oriented at (45°/135°) to load direction.

To compare the different retrofit schemes, identical As-built (Series **A**) specimens were constructed and tested under the same conditions as Series **R** specimens. This brings the total to 18 intersecting wall specimens 15 retrofitted (R Series) and 3 unretrofitted (A Series).

Material Properties

Nominal 25 MPa (40 20 20 cm) standard hollow concrete masonry blocks certified to meet the provisions of ASTM C-90-06b standard and Type S mortar (ASTM C-270) was used in the construction of the walls. The GFRP had 0.915 kg/m^2 of E-glass fibers in the form of woven fabric in one direction with roving in the orthogonal direction as weft to stabilize the fabric. The properties of the GFRP composites, given in Table 1, determined according to ASTM D-3039 specification, were supplied by the manufacturer. A detailed study conducted by El-Dakhakhni et al. (2004) evaluated the effect of different GFRP laminates on the behaviour of masonry assemblages and concluded that the use of the GFRP laminate, similar to the one used in the current study, was most effective in preventing in-plane shear failure of the tested specimens. All specimens were constructed with face shell mortar bedding [i.e. mortar on only the face shell of the block was used]. The mortar joints were tooled to produce a concave profile. The tooling produces a denser compacted surface and forces the mortar into tight contact with the masonry units. The mortar mix prepared met ASTM C270-07 specifications. The average mortar strength was found to be 22.2 MPa with a 9.0% COV. Three 50 mm mortar cubes were taken from each mortar mix and tested for compressive strength as per ASTM C-109/ C109M-05. Commercially available TTJR that conformed to MSJC (2005) and CSA S304.1 requirements were used. The mechanical properties of the TTJR, as determined per ASTM A82/ A82-05a, are shown in Table 2.

Table 1: Glass Fiber-Reinforced Polymer Composites and Dry Fibers Properties

Composite laminate properties		Dry fiber properties	
Ultimate tensile strength in primary fibers direction (MPa)	575	Tensile strength(GPa)	3.24
Elongation at break (%)	2.2	Ultimate Elongation (%)	4.5

Tensile Modulus (GPa)	26.1	Tensile Modulus (GPa)	72.4
Ultimate tensile strength 90° to primary fibers direction (MPa)	25.8	Density (g/cm^3)	2.55
Laminate thickness (mm)	1.3	Weight (g/m^2)	915

Table 2: Truss-Type Reinforcement Size and Properties

	Longitudinal Wires properties	Cross Wire properties
Wire Diameter(mm)	4.76	3.66
Cross-sectional area per wire (sq.mm)	17.80	10.52
Yield strength (MPa)	482.6	482.6
Tensile strength (MPa)	551.58	551.58

Test Setup and Instrumentation

The choice of loading assembly was based on work done by Drysdale et al. (2008). All of the assemblages utilised the same loading assembly as described herein. Figure 4 shows the typical test set-up. The specimens were loaded using a displacement-controlled actuator and loads were recorded using a 400 kN load cell. A spreader beam in conjunction with roller supports was used to transfer loads from the actuator to the web of the specimen as close as possible to the flange-web intersection (see Fig. 4). Locating the loading plates and support rollers as close as possible to the flange-web intersection facilitated subjecting the specimen to a state of nearly pure shear by minimizing additional flexural stresses across the interface due to eccentricities. The steel bearing plate located under the loading and above the support rollers was used to prevent local bearing failure mode. Specimens were placed on a hydrostone bed on the testing floor. Four LPDTs (Linear Potential Displacement Transducers) were placed on the assemblage as shown in Fig. 4. The LPDTs & load cell were connected to a PC Data acquisition system. Two LPDTs were located on the ADL floor to measure vertical displacement of the web near the flange-web intersection. The other two LPDTs measured any possible horizontal displacement at the intersection. The two vertical LPDTs had a 25.4 mm nominal gauge length and the two horizontal LPDTs had a 12.7 mm nominal gauge length respectively.

Preparation of Test Specimens

The construction of wall specimens was performed by the same skilled mason within one week to minimize the effect of workmanship on altering the results. All specimens tested for the scope of this project required two TTJR per specimen crossing each flange-web intersection. The horizontal TTJR welded tees were located in the bed joints with only face shell bedding. Because of the short web length (one block long), the manufacturer-supplied TTJR tees had to be trimmed, to limit more than one tee crossing a flange-web intersection. Figure 4 shows the location of the TTJR tees on the third course from the bottom of the specimens. However, even though there was overlapping of tees in the web area of the specimen, only one tee was allowed to cross the flange-web intersection.

This simplified the interpretation of the results and reflected actual construction as well.

Specimens were constructed according to common practice in North America with face shell bedding, no re-tempering of the mortar was allowed and all mortar joints were tooled to a concave profile. All specimens were air cured for at least 90 days before testing. Wood spacers and stretcher units were located directly under the web during construction to behave as temporary shoring until the mortar cured and to prevent any premature web slippage. The stretcher unit and wood spacers were removed after curing to allow for installation of LPDTs to measure vertical displacements.

Three of the 18 specimens were not retrofitted to be tested as the control specimens, the remaining 15 were retrofitted with GFRP Composite laminate using different schemes according to the following application procedure. The epoxy mix was prepared per the manufacturer's specification for mix-ratio and mixing procedure. Specimen surfaces were first wire brushed and vacuumed for dust to get proper bonding surface. The epoxy moisture was applied on the pre-cut fabrics with a paint roller on each side. The saturated fibers were then applied on to the specimen surface and more epoxy was applied as required to ensure proper bond between the composite laminate and the concrete masonry substrate. Proper bond, especially near the intersection, was ensured by manually squeezing out any trapped air voids or excess epoxy. Retrofitted specimens were allowed to air cure for a minimum of 72 hours before testing per the manufacturer's specifications.

TEST RESULTS AND DISCUSSION

The test results are summarized in Table 3, and discussed in the following section with respect to failure modes, strengths, and deformation characteristics.

Table 3: Experimental Results of Test Specimens

Series	Specimen #	Failure Load, P (kN)	Vertical slip at ultimate load (mm)	Average failure Load (kN)	Standard Deviation (kN)
A	1	41	4.46	47	5
	2	51	9.36		
	3	48	1.17		
R90°	1	106	2.07	97	10
	2	99	1.00		
	3	86	1.17		
R0°	1	94	1.53	89	10
	2	96	9.63		
	3	78	1.10		
R90°/0°	1	148	2.12	142	7
	2	144	8.35		
	3	136	1.78		
R(90°/0°)^2	1	233	1.90	229	4
	2	226	9.23		
	3	228	2.87		
R45°/135°	1	214	1.32	214	15
	2	229	1.43		
	3	199	1.95		

Series A:

Failure Modes: Initial failures of all three as-built specimens were characterized by a shear-slip failure along the block-mortar interface at the flange-web intersection [Fig. 6(a)]. This slip did not occur simultaneously on both sides of the web. After initial slippage, the specimens exhibited significant post-slip capacities. Final failure was characterized by a snapping noise indicating failure of the TTJR. Closer inspection of deformed truss revealed two types of failure [Fig. 6(b)] in the TTJR: yielding of the longitudinal rods of the truss or fracture of the weld at the intersection of the longitudinal and diagonal truss members. One of the three specimens suffered spalling of the concrete near the intersection [Fig. 6(c)].

Strength Characteristics: For the A-Series specimens, the initial capacity was provided by the shear strength of the mortar at the intersection. Once cracking and slippage occurred there was a temporary reduction in load carrying capacity as indicated by the descending trend in Fig. 7. With further web displacements, substantial load carrying capacity developed as indicated by the ascending portion of the load-displacement curve in Fig. 7. The residual load-carrying capacity post-slippage is attributed to the shear friction along the failure surface as proposed by Drysdale et al. 2008. Essentially as the web displaced downwards, the TTJR was engaged and began to deform, and, subsequently, was subjected to tension. The horizontal component of this tension force multiplied by the coefficient of friction at the web-flange intersection, resulted in a vertical force opposite to the applied load [Fig. 5]. At some instances the post-slip capacities exceed the initial peak capacities; however the gain in strength was nowhere near the pre-slip peak value. This can be seen in Fig. 7 for Specimen A-3(see bold line). The average ultimate capacity of the three A-Series specimens was 47.0 kN [Table 3].

Deformation Characteristics: A typical load-displacement relationship for Series-A is shown in Figure 7 (see bold line). A linear load-displacement relationship from point *a* to ultimate load (point *b*) is visible. Beyond point b, shear-slip occurred via cracking of the flange-web mortar interface. This can be seen by the stiffness degradation on the graph from point *b* to *c*. After the shear-slip crack, a load reduction to point *c* can be noticed. However, a gain in stiffness from point *c* to *d* resulted in capacity increase (post-slip maximum load) but it was still well below peak pre-slip load. Continued displacements, resulted in a decreasing load carrying capacity due to the yielding of the TTJR, therefore no other sources of strength existed in the A-Series specimens. The average recorded pre-slip displacement was 0.86 mm and the average residual post-slip displacement was 5.63 mm as can be seen in Fig. 19.

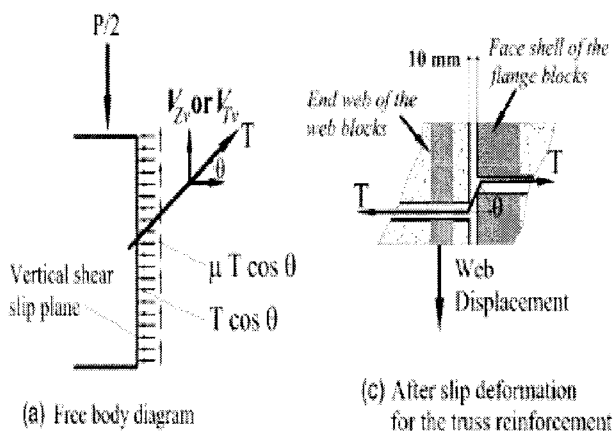

Figure 5: Truss reinforced specimen behaviour proposed by Drysdale et al. (2008)

T = tension force developed by the reinforcement crossing the intersection

V_{Tv} = vertical component of the truss reinforcement tensile force in the deformed position

θ = angle of reinforcement crossing flange-web intersection after shear slip

μ = coefficient of friction.

(a)
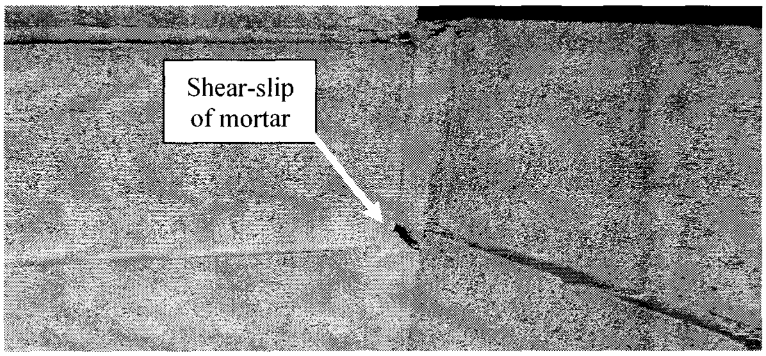

(b)
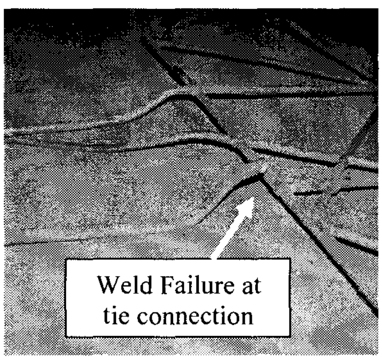

(c)
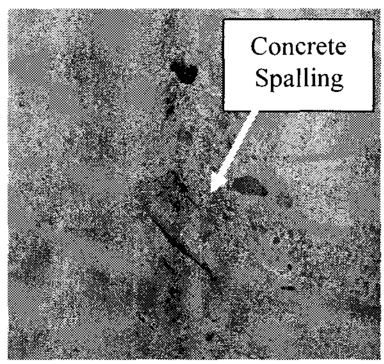

Figure 6: Failure modes-Series A specimens: (a) Shear slip of mortar, (b) Weld Fracture, and (c) Spalling of concrete

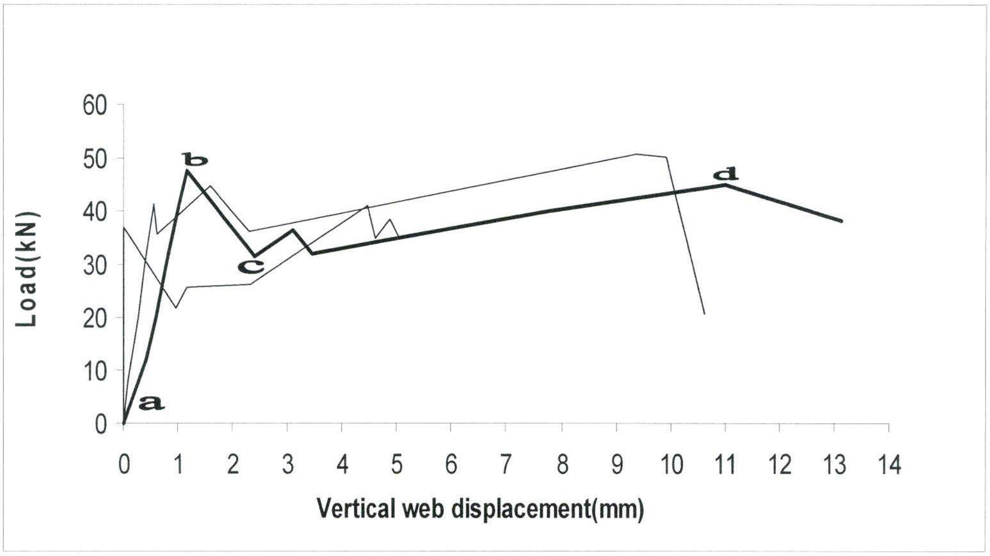

Figure 7: Load vs. displacement relationship for Series **A** specimens

Series R0º

Failure Modes: Initial failure was indicated by tearing [Fig. 8] of the FRP laminate sheet in the vicinity of the flange-web intersection. This type of failure was also reported by Ehsani (1997) and El-Dakhakhni et al. (2004). Final failure was characterized by a snapping noise indicating failure of steel TTJR. Closer inspection of the deformed truss members showed, again, two types of failure [Fig. 6(b)] in the TTJR: yielding of the longitudinal rods of the truss or fracture of the weld at the intersection of the longitudinal and diagonal truss members.

Strength Characteristics: Four sources of strength available for assemblages with the above mentioned retrofit scheme are shear strength of mortar, composite laminate strength and steel reinforcement induced shear friction caused by the elongation of the steel truss members. Unlike the A-Series, initial resistance of Series R0° to applied load was supplied by the shear strength of the mortar and the stabilizing weak fibers (oriented orthogonally to load direction) which later sheared-off as expected. The composite system provided the intersection with an increased load carrying capacity [Fig. 19] and stiffness by delaying the shear-slip of the mortar at the intersection. After slip, any residual capacity was provided by the steel TTJR and the induced shear friction mobilized by the elongation of the steel rods.

In retrospect, orienting unidirectional fibers parallel to load direction seems inefficient because any resistance by the laminate would be offered by the shearing of the epoxy and fibers in the weak direction. In addition, tearing of the laminate is a fairly brittle failure mode compared to delamination and other failure modes observed in other specimens as will be shown later. The average load carrying capacity of the assemblages tested in this phase was 97 kN [Table 3], almost twice the capacity of the A-Series [Figure 20].

Deformation Characteristics: The load-displacement relationship of assemblages tested for this phase is shown in Fig. 9, with a typical relationship (for Specimen Series R0°-2) shown in bold. From the graph, the load-displacement relationship is linear up to maximum load (point *b*) is visible. From point *b* to *c*, the slipping of the web is observable. It is believed that, the FRP resulted in this stiffness enhancement and in the delay of the shear-slip of the mortar at the flange-web intersection.

However, because the main fibers were not engaged in resisting the shear due to their orientation, no further residual capacity was available. Therefore a decreasing trend is noticed from point *b* to *c*. Continued displacements, resulted in a gain in load carrying capacity attributed to the deformation of the steel rods in the TTJR. This increase in stiffness occurred up to point *d*. A decreasing load carrying capacity due to the yielding of the longitudinal steel ties occurred at point *d*, therefore no other sources of strength remain in the A-Series specimens. The average recorded displacement at maximum load was 1.41 mm as shown in Fig. 19.

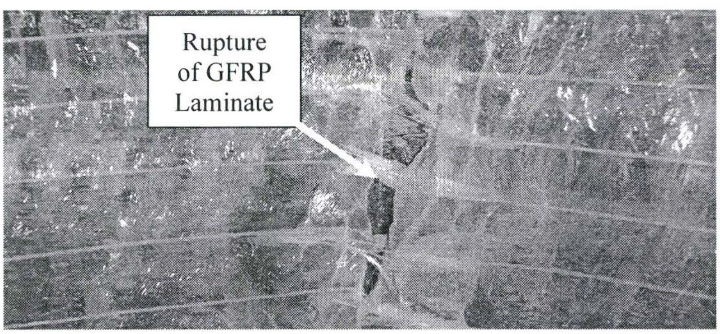

Figure 8: Failure mode – Series **R0°**

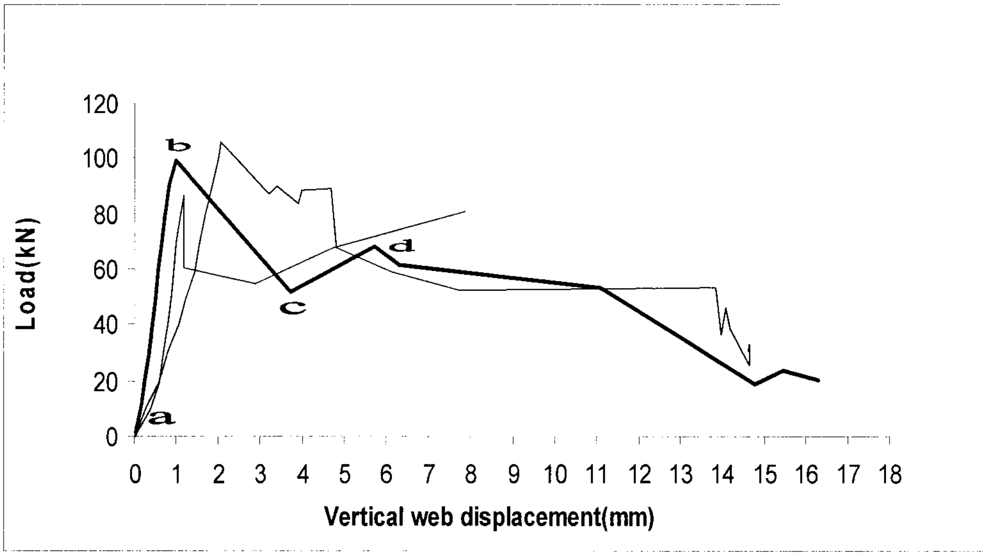

Figure 9: Load vs. displacement relationship for Series **R0**° Specimens

Series R90°

Failure Modes: Similar to the previous specimens, the initial failure for the specimens tested in this phase was a shear-slip along the vertical flange-web intersection. However, unlike Series R0° specimens, the GFRP provided residual post-slip capacity. At times, the post-slip peak load was higher than the pre-slip peak load. The FRP failure mode was a partial delamination in the vicinity of the vertical intersection. However, because the fibers were not able to sustain shear deformations, the failure mode for the laminate system was similar to that of dowels as shown in Fig. 10. Ultimate failure was characterized by snapping of the steel rods.

Strength Characteristics: The load-displacement relationship of assemblages tested for this phase is shown in Fig. 11, with a typical relationship (for Specimen Series R90^{o}-2) shown in bold. Comparing the pre-slip load-displacement trend for Series R0^{o} and R90^{o} in Fig.19 provides two valuable observations. First, the peak-load was roughly the same for both phases, indicating that the resistance may have been provided by the shear strength of the epoxy layer of the laminate system and the mortar at the intersection. Secondly, the stiffness of the specimens was almost identical up to peak load for both phases. However, the major improvement that specimens of this series achieved was the enhancement to the post-peak behavior compared to Series R0^{o} specimens. This will be discussed in the following section under deformation characteristics. After undergoing large displacements, resistance to applied load was supplied by the TTJR due to elongation based on the same mechanism as explained earlier. The average ultimate capacity of the three specimens tested was 89 kN [Table 3]. An increase of 1.91 times its unretrofitted specimen's capacity [Figure 20].

Deformation Characteristics: A typical load-displacement relationship is that of Specimen Series R90^{o}-2 shown in Fig. 11. The relationship is almost linear (*a* to *b*) up to the pre-slip peak load. After shear-slip, the load carrying capacity decreased up to point *c*. After sufficient deformation had occurred, the fibers within the FRP laminate were engaged. From point *c* to *d*, one can notice the substantial post-peak residual capacity. In addition, a ductile failure mode, as indicated by the plateau (*c* to *d*) was achieved. This enhancement to the post-peak behavior is attributed to the fact that the FRP fibers had to deform from its 90° orientation to provide any resistance to applied load. This is confirmed by observing Fig. 11, where one can notice that with increasing displacement, there was a progressive degradation of stiffness from point *c* to *d*, indicating fibers undergoing dowel action and re-orienting with increased specimen capacity. In Fig. 19, comparing the typical load-displacement trend of Series R90° and R0° it can be noticed that both series are almost identical up to a displacement of approximately 5.0 mm. However, after 5 mm, Series R0° specimens experienced a continuous degradation of stiffness after reaching pre-slip peak load. The fiber re-orientation of Series R90° specimens resulted in an improved pseudo-ductile behaviour, as indicated by the plateau in Fig. 19. Comparison between Series R90° and R0° demonstrates the importance of fiber orientation on the post-peak behavior of the retrofitted specimen. The average recorded pre-slip displacement was 1.2 mm and the average residual post-slip displacement was 4.1 mm [Fig. 19].

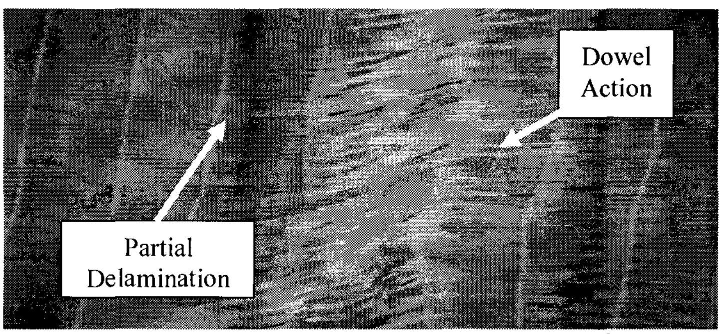

Figure 10: Failure mode – Series **R90°**

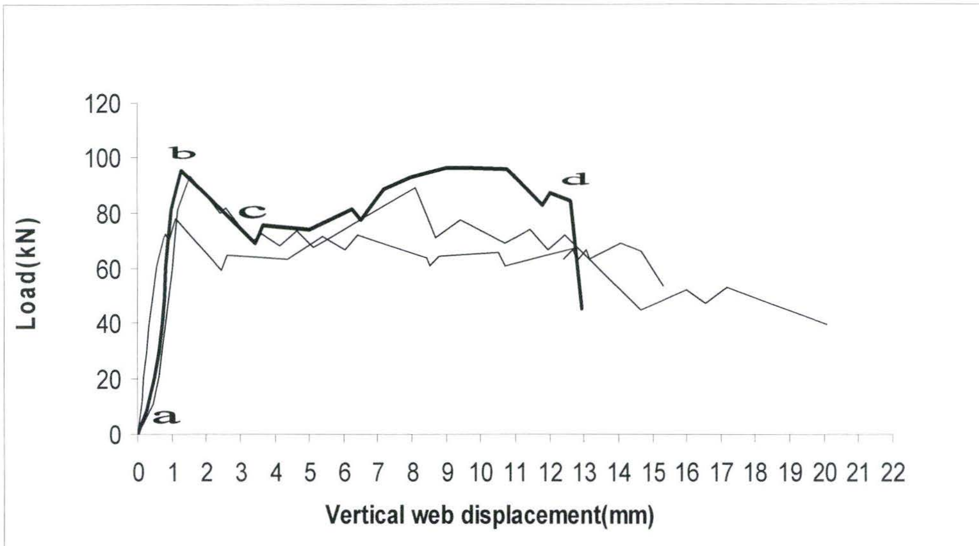

Figure 11 : Load vs. displacement relationship for Series **R90°** Specimens

Series R90°/0°

Failure Modes: Using two orthogonal layers of the unidirectional fibers meant that vertical deformation of the horizontal fiber engages the connected vertical fiber into tension; thus resulting in a diagonal tension state (see Fig. 12) of stress in the laminate system.

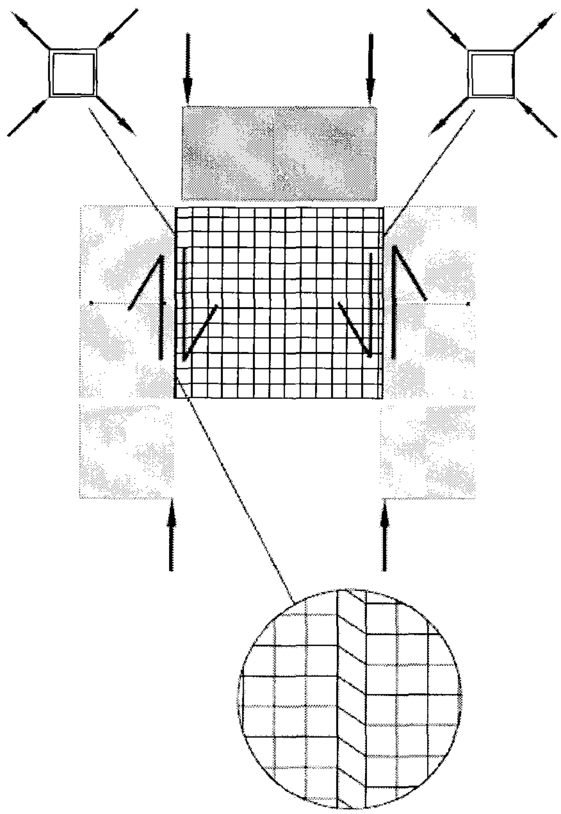

Figure 12 : The two diagonal tension fields

Initial failure for specimens associated with this phase of testing was characterized by a shear-slip along the flange-web intersection of the composite assemblage. Unlike Series R0° specimens, the tearing of the laminate was not sudden. Failure of the laminate commenced with partial tearing followed by partial delamination and was concluded by complete tearing of laminate system [Fig 13]. Failure modes exhibited by this series were combinations of those sustained by Series R0° and R90° specimens. As expected, final failure was characterized by a snapping noise indicating failure of steel TTJR.

Strength Characteristics: Application of two layers of laminate provided the assemblage with improved performance compared to those of Series R0^{o} and R90^{o}. The maximum average load achieved for specimens in this phase was roughly 50% more [Table 3] than those of Series R0^{o} and R90^{o}. Sufficient epoxy bond strength was available to transfer stresses from the 1st laminate layer to the next. Therefore under sustained loading, the load path was provided by the 90^{o} laminate of the base layer displacing vertically and engaging the strong horizontal fibers to undergo dowel action similar to Series R90^{o}. Moreover, the shear friction component of this force helped improving the specimen resistances. The vertical displacement also resulted in the partial tearing of the composite laminate system. Once partial delamination and/or tearing occurred, transfer of forces to the steel TTJR resulted, ultimately, in their failure. The average ultimate capacity of Series R90^{o}/0^{o} specimens tested was 142 kN [Table 3], approximately 3 times Series A specimen's capacity [Figure 20].

Deformation Characteristics: The load-displacement curve of Specimen R90^{o}/0^{o}-2, shown in Fig. 14(bold line), indicates that the stiffness of the assemblages tested in the phase is almost constant and linear from point *a* to point *b*. From *a* to *b*, the laminate was able to improve the stiffness of the intersection, thus delaying the shear-slip of the mortar at the intersection. Stiffness degradation occurred after achieving a peak load, indicating slipping of the web up to point *c*. After sufficient deformation occurred, a positive stiffness resulted in a new post-slip peak load (point *d*). This residual capacity was offered by the dowel action of individual horizontal fibers of the 90° GFRP layer. There was a progressive degradation of stiffness, just as experienced by the composite assemblages of Series R90°. Large deformations resulted in the steel ties getting engaged into tension and causing final failure through yielding and fracture.

Comparison between pre-slip load-displacement [Fig. 19] trend for Series R90°/0° to that of R0° and R90° indicated the following observations: the use of the bi-directional laminate resulted in improved pre-slip stiffness of the wall specimen. In addition, the horizontal fibers directly affect the pseudo-ductility of the composite assemblage. The average recorded pre-slip displacement was 1.33 mm and the average residual post-slip displacement was 4.08 mm [Fig. 19].

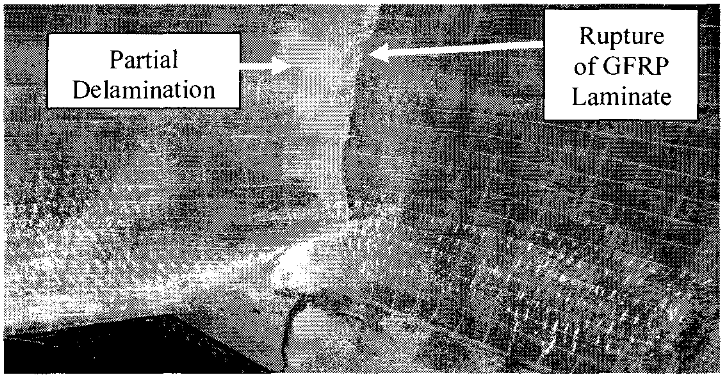

Figure 13: Failure mode – Series **R90°/0°**

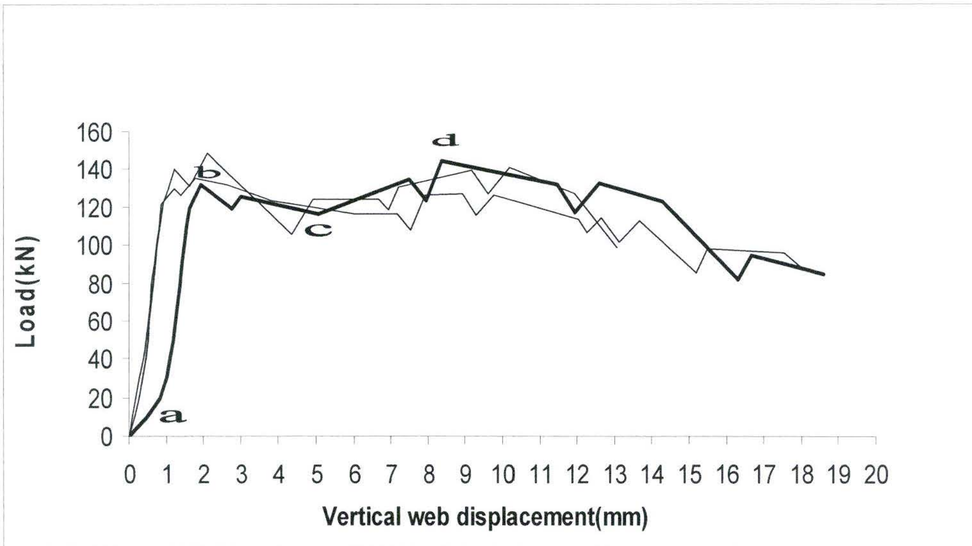

Figure 14: Load vs. displacement relationship for Series **R90°/0°** Specimens

Series R(90°/0°)²

Failure Modes: Initial failure of this series was also a shear-slip of the mortar at the flange-web intersection. Doubling the thickness of GFRP aimed at eliminating the vertical tearing of laminate as a governing failure mode, since it is brittle in comparison to delamination. However, the final failure mode achieved in this series was of a brittle nature through formation of a crack through the webs of the blocks and ultimately tensile splitting of the concrete masonry units(CMU) through the faceshells (see Fig. 15). The splitting of the CMU is due to the induced lateral tensile stresses developed in the laminates, which resisted the vertical displacement of the web block relative to the flange at the intersection. This shows the implication of increasing the laminate density on altering the failure mode of composite retrofitted walls. Unlike the previous retrofit schemes, the steel TTJR did not fail since failure was caused by masonry failure as will be discussed in the following section.

Strength Characteristics: The strength of the composite assemblage was controlled by the tensile splitting strength of concrete masonry unit (CMU). This is due to the interfacial stress between the GFRP laminate and the concrete masonry units. The stronger GFRP and the epoxy bond between the laminate and concrete block was sufficiently high to eliminate tearing as the predominant failure mode as observed in the previous phases of the project. Application of load causes the laminates fibers to go into tension, causing a tensile force on the faceshell of the concrete blocks.

The double thickness of GFRP laminate ensured that none to very little shear deformation occurred. The GFRP laminate was able to improve the strength and stiffness of the mortar joint, thus delaying the onset of shear-slip. Therefore, the critical weak link was the concrete block itself. Due to the high stiffness of the specimens, very little deformation occurred; therefore the concrete block was not able to engage the TTJR. Therefore, only sources of the strength were the mortar along the vertical intersection, laminate system and the concrete block itself.

The average ultimate capacity of the three specimens tested was 229 kN [Table 3], approximately 4.91 times Series A specimen's capacity [Fig. 20].

Deformation Characteristics: The average load-displacement relationship of R($90^o/0^o)^2$-1, shown in Fig. 16(bold line) can be considered typical for the discussion of this section. The load-displacement relationship was linear up to the peak load (point *b*) as can be seen in Figure 16. After achieving peak load the assemblages were not able to sustain this load level for increasing deformation. Even though the specimens of this phase were the strongest among the entire retrofit schemes, Fig. 19, shows that the load-displacement relationship was considerably more brittle than the previously tested phases. Point *c* represents failure when the faceshells within the CMU split and testing was terminated. Figure 19, also shows the improved stiffness of the double thickness laminate system which was able to delay the shear-slip of the mortar at the flange-web intersection. The average recorded displacement at peak load was 4.66 mm [Fig. 19].

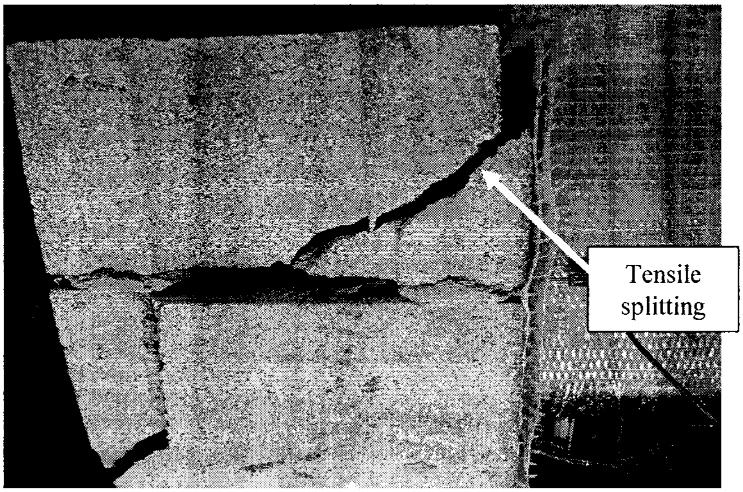

Figure 15: Failure mode – Series **R ($90^o/0^o)^2$**

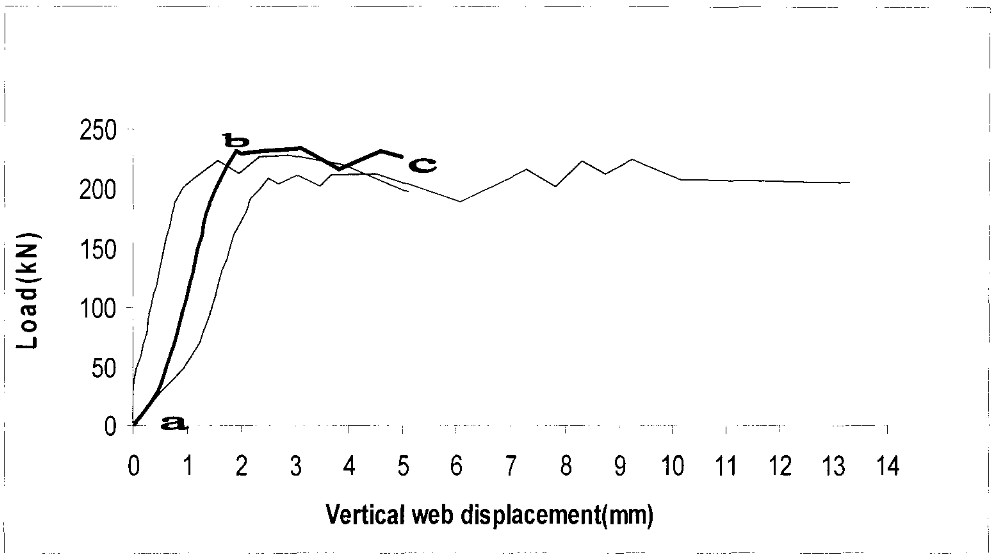

Figure 16: Load vs. displacement relationship for Series **R $(90^o/0^o)^2$** Specimens

Series R45°/135°

Failure Modes: The failure mode for the specimens associated with the retrofit scheme employed in this phase was of complete delamination of the laminate at either side of the intersection [Fig. 17]. This was followed instantaneously by the yielding of the steel ties. This can be attributed to the transfer of stresses from the laminate system to the only remaining source of strength of the assemblage which are the steel ties. Shear-slip of the mortar at the intersection would have occurred prior to the transfer of stresses to the steel ties.

Strength Characteristics: The orientations of the fibers selected in this phase prove to be an efficient means of increasing the strength of the composite assemblage. For the same fabric density, specimens of series R45°/135° were able to achieve average peak loads 1.5 times that of the R90°/0° [Table 3]. This can be explained due to the higher stiffness of the laminate system; which is attributed to the fibers being subjected to direct tension. The average ultimate capacity of the three specimens tested was 214 kN [Table 3], an average increase of 4.6 times Series A specimen's capacity [Fig. 20].

The fibers oriented at 45 ° to the loading plane are subjected to axial tension. However, orienting unidirectional fibers at 135 ° to the plane of loading seems inefficient because any resistance by the laminate would be offered by the axial compression of the strong fibers. GFRP Laminates are utilized for their strength in tension and not compression. However, the assemblage being tested in a full-scale wall would require fibers oriented in both directions due to the possibility of load reversal when subjected to a seismic load. Therefore, to represent in-situ conditions, the assemblages of this series were retrofitted with unidirectional fibers at 45° and 135 ° to the loading plane.

Deformation Characteristics: The load-displacement curve of Specimen R45°/135°-2, shown in Fig. 18(bold line), indicates that the stiffness of the assemblages tested in the phase is almost constant and linear from point *a* to point *b*. Beyond point *b*, the specimens exhibited almost perfect brittle failure. Specimens of this series exhibited almost constant stiffness up to failure (point *b*). An important observation here is the impact of fiber orientation on the deformation characteristics of the assemblage. The orientations of the fibers selected in this phase prove to be supply the highest stiffness most efficiently among all the retrofit schemes tested. This can be seen in Figure 21, where the single thickness of FRP laminate in the R45°/135° series had as much stiffness as the double thickness of FRP laminate used in the R $(90°/0°)^2$ series. However, on average, the displacements at ultimate load for Series R45°/135° specimens were 38 % that of the specimens tested in Series R90°/0°. The average recorded displacement at peak load was 1.56 mm [Fig. 19].

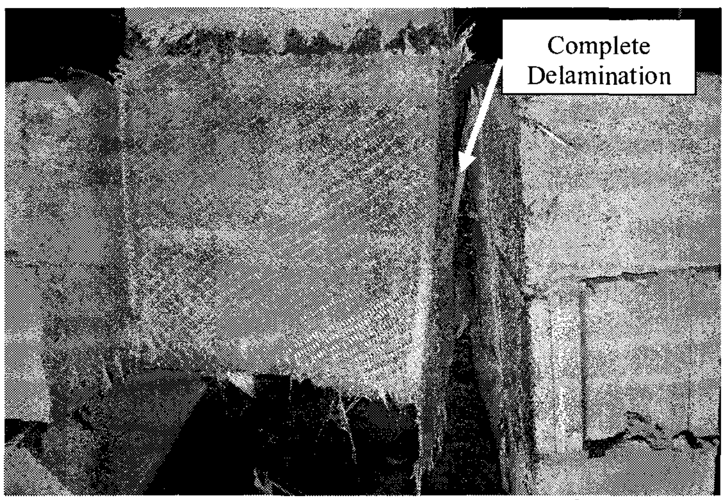

Figure 17: Failure mode – Series **R45°/135°**

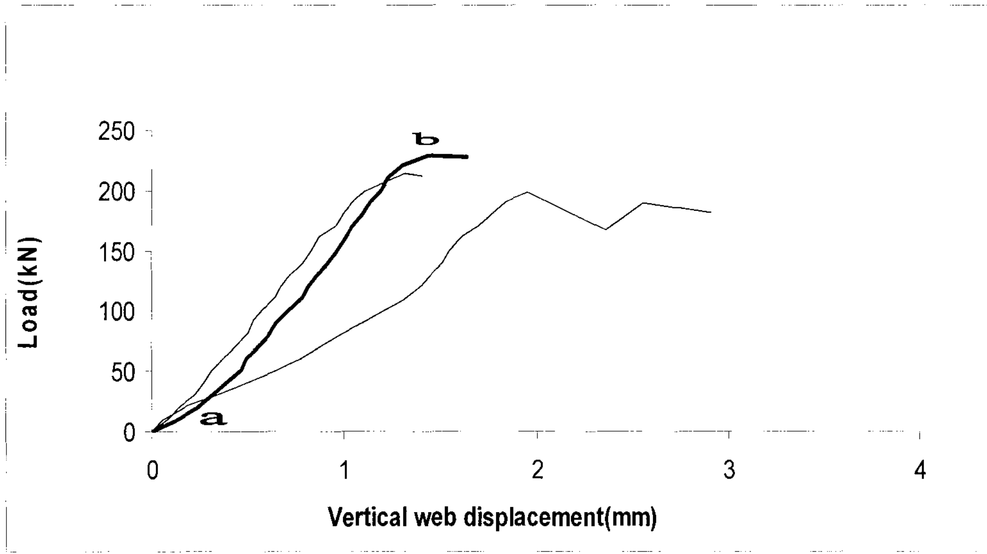

Figure 18: Load vs. displacement relationship for Series **R45°/135°** Specimens

CONCLUSIONS

Three unretrofitted and fifteen retrofitted intersecting masonry assemblages were tested under different retrofit schemes. Tests included assemblages retrofitted with unidirectional fibers (0°), unidirectional fibers (90°), bidirectional fibers (90°/0°), bidirectional fibers (90°/0°) – Double thickness & bidirectional fibers (45°/135°) subjected to direct shear at the flange-web intersection. The following conclusions were derived from the exploratory investigation:

1. The GFRP laminates increased the load-carrying capacity of the intersecting masonry assemblages, exhibiting shear-failure of the vertical mortar joint (as-built), tearing of the FRP laminate (0°), partial delamination (90°), a combination of tearing and delamination (0°/90°),

tensile splitting of the concrete block (Double thickness- $0^{o}/90^{o}$), & complete delamination of GFRP laminate($45^{o}/135^{o}$). Increase in shear strength capacity varied from 1.91 to 4.91 times the as-built specimens [Fig. 20].

2. Assemblages retrofitted with GFRP strong fibers oriented orthogonally to load direction (Series R90^{o}) prove to improve the post-peak behaviour the most by providing some kind of pseudo-ductility [Fig. 19].
3. The single layer of GFRP with strong fibers oriented ($45^{o}/135^{o}$) to load direction prove to be most efficient in improving the stiffness of the composite assemblage prior to shear-slip of the vertical mortar joint [Fig. 21].
4. Fabric density had a direct impact on strength & altering the failure mode from the GFRP laminate system to the concrete block.
5. Fabric orientation proves to directly affect strength and stiffness of the composite assemblage [Figure 20 and Figure 21].
6. Depending on service use; density and orientation can be adjusted to improve the strength, post-peak behaviour and stiffness of intersecting shearwalls. The GFRP laminate system has helped to improve the performance of the as-built specimens and address the need for the seismic retrofit of intersecting shear walls.

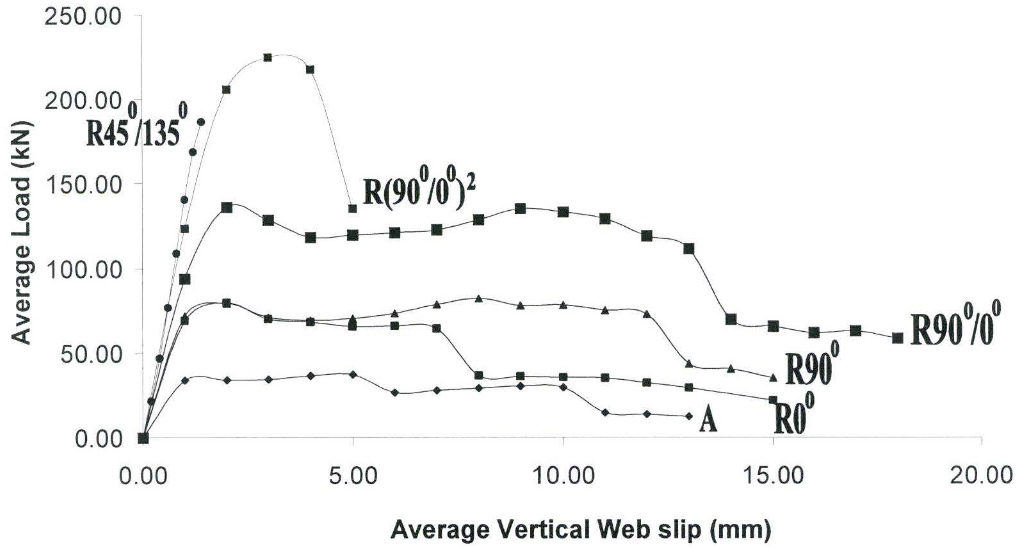

Figure 19: Load vs. displacement relationship (averaged) for different series specimens

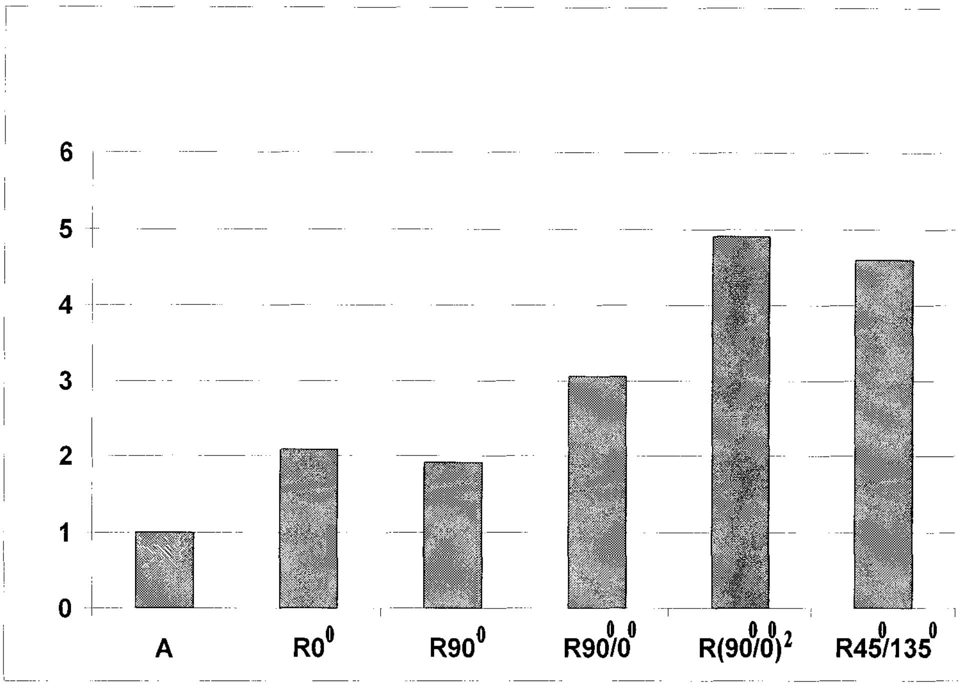

Figure 20: Variation of shear strength of various retrofit series compared to as-built specimens

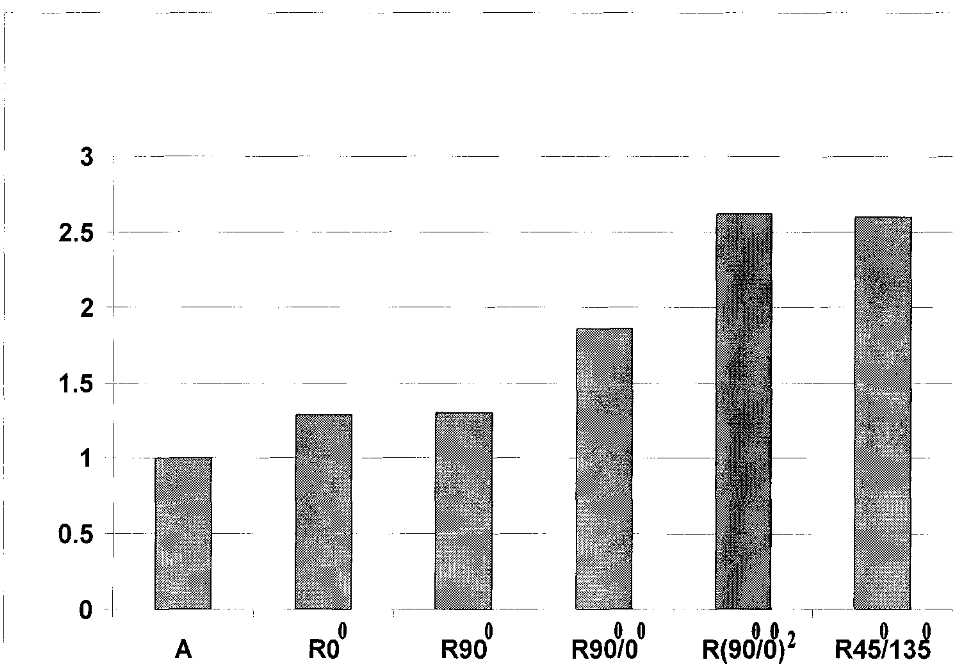

Figure 21: Variation of pre-slip stiffness of various retrofit series compared to as-built specimens

NOTATION

The following symbols are used in this paper:

FRP	=	Fiber-Reinforced Polymer
GFRP	=	Glass Fiber-Reinforced Polymer
TTJR	=	Truss-Type Joint Reinforcement
COV	=	Coefficient of Variation
LPDT	=	Linear Potential Displacement Transducers
CMU	=	Concrete Masonry Units

REFERENCES

Albert, M. L., Elwi, A. E., and Cheng, J. J. R. (2001). "Strengthening of unreinforced masonry walls using FRPs." *J. Compos. Constr.*, 5(2), 76–84.

American Society for Testing and Materials (ASTM). (2005a). "Standard specification for steel wire, plain, for concrete reinforcement." *A82/ A82M-05a, Annual book of ASTM standards*, Vol. 01.04, West Conshohocken, Pa.

American Society for Testing and Materials (ASTM). (2005b). "Standard test method for compressive strength of hydraulic cement mortars." *C109/C109M-05, Annual book of ASTM standards*, Vol. 04.01, West Conshohocken, Pa.

American Society for Testing and Materials (ASTM). (2006). "Standard specification for load-bearing concrete masonry units." *C 90-06b, Annual book of ASTM standards*, Vol. 04.05, West Conshohocken, Pa.

American Society for Testing and Materials (ASTM). (2007). "Standard specification for mortar for unit masonry." *C 270-07, Annual book of ASTM standards*, Vol. 04.05, West Conshohocken, Pa.

American Society for Testing and Materials (ASTM). (2006). "Standard Test Method for Tensile Properties of Polymer Matrix Composite Materials." D-3039, *Annual book of ASTM standards*, West Conshohocken, Pa.

BLOK-LOK Ltd. (2007, online): Available: www.blok-lok.com

Canadian Standards Association (CSA). (2004a). "Masonry design and construction for buildings." *S304.1*, Canadian Standards Association, Rexdale, Ontario, Canada.

Canadian Standards Association (CSA). (2004b). "Standards on concrete masonry units." *A165-04*, Canadian Standards Association, Rexdale, Ontario, Canada.

Drysdale, R.G., Hamid, A. and Baker, L.R. (1999). Masonry Structures: Behavior and design, 2nd Ed., Masonry Society, Boulder, Colorado.

Drysdale, Robert G., El-Dakhakhni, Wael W. and Kolodziejski, Edward A. (2008). "Shear Capacity for Flange-Web Intersection of Concrete Block Shear Walls." *Journal of Composites for Construction, ASCE, Vol. 134, No.6, June, pp.947-960, 2008.*

Ehsani, M.R., Saadatmanesh, H. and Al-Saidy, A. (1997). "Shear Behaviour of URM Retrofitted with FRP Overlays," *Journal of Composites for Construction, ASCE, Vol. 1, No. 1, February, pp. 17-25, 1997.*

El-Dakhakhni, Wael W., Hamid, Ahmad A. and Elgaaly, Mohamed. (2004). "In-Plane Strengthening of URM Infill Wall Assemblages using GFRP Laminates." *TMS Journal, September, Boulder, Colorado. Pp. 13-24, 2004.*

Fyfe Co. LLC (2008, online): Available: www.fyfeco.com

Hamid, Ahmad A., El-Dakhakhni, Wael W. and Hakam, Zeyad H.R. (2005). "Behaviour of Composite Unreinforced Masonry-Fiber-Reinforced Polymer Wall Assemblages Under In-Plane Loading." *Journal of Composites for Construction, ASCE, Vol. 9, No. 1, February, pp.73-83, 2005.*

Hamilton, III, H. R., and Dolan, C. W. (2001). "Flexural capacity of glass FRP strengthened concrete masonry walls." *J. Compos. Constr.*, 5(3), 170–178.

Hamoush, S. A., McGinley, M. W., Mlakar, P., Scott, D., and Murray, K. (2001). "Out-of-plane strengthening of masonry walls with reinforced composites." *J. Compos. Constr.*, 5(3), 139–145.

Kuzik, M. D., Elwi, A. E., and Cheng, J. J. R. (2003). "Cyclic flexure tests of masonry walls reinforced with glass fiber reinforced polymer sheets." *J. Compos. Constr.*, 7(1), 20–30.

Masonry Standards Joint Committee (MSJC). (2005). "Building code requirements for masonry structures." *ACI 530-05*, *ASCE 5-05*, *TMS 402-05*, American Concrete Institute, Detroit, Mich., American Society of Civil Engineers, Reston, Va., Masonry Society, Boulder, Colo.

Paulay, T., and Priestley, M. J. N. (1992). *Seismic design of reinforced concrete and masonry buildings*, Wiley, New York.

Tan, K. H., and Patoary, M. K. H. (2004). "Strengthening of masonry walls against out-of-plane loads using fiber-reinforced polymer reinforcement." *J. Compos. Constr.*, 8(1), 79–87.

Triantafillou, T. C. (1998). "Strengthening of masonry structures using epoxy-bonded FRP laminates." *J. Compos. Constr.*, 2(2), 96–104.

Velazquez-Dimas, J. I., and Ehsani, M. R. (2000). "Modeling out-of plane behavior of URM walls retrofitted with fiber composites." *J. Compos. Constr.*, 4(4), 172–181.

APPENDIX A: MATERIAL DATA SHEETS

FYFE Co. LLC
Tyfo® Fibrwrap® Systems

Tyfo® SEH-51A Composite
using Tyfo® S Epoxy

DESCRIPTION
The Tyfo® SEH-51A Composite is an ICC ER-2103 listed material comprised of Tyfo® S Epoxy and Tyfo® SEH-51A reinforcing fabric. Tyfo® SEH-51A is a custom weave, uni-directional glass fabric used in the Tyfo® Fibrwrap System. The glass material is orientated in the 0° direction with additional yellow glass cross fibers at 90°. The Tyfo® S Epoxy is a two-component epoxy matrix material.

USE
Tyfo® SEH-51A Fabric is combined with Tyfo® epoxy material to add strength and ductility to bridges, buildings, and other structures.

ADVANTAGES
- ICC-ES ESR-2103 listed product
- Component of UL listed, fire-rated assembly
- NSF/ANSI Standard 61 listed product for drinking water systems
- Good high & low temperature properties
- Long working time
- High elongation
- Ambient cure
- 100% solvent-free
- Rolls can be cut to desired widths prior to shipping

TYPICAL DRY FIBER PROPERTIES	
Tensile Strength	470,000 psi (3.24 GPa)
Tensile Modulus	10.5×10^6 psi (72.4 GPa)
Ultimate Elongation	4.5%
Density	0.092 lbs./in.^{3} (2.55 g/cm^3)
Weight per sq. yd.	27 oz. (915 g/m^2)

COMPOSITE GROSS LAMINATE PROPERTIES

PROPERTY	ASTM METHOD	TYPICAL TEST VALUE	DESIGN VALUE*
Ultimate tensile strength in primary fiber direction, psi	D-3039	83,400 psi (575 MPa) (4.17 kip/in. width)	66,720 psi (460 MPa) (3.3 kip/in. width)
Elongation at break	D-3039	2.2%	1.76%
Tensile Modulus, psi	D-3039	3.79×10^6 psi (26.1 GPa)	3.03×10^6 psi (20.9 GPa)
Ultimate tensile strength 90 degrees to primary fiber, psi	D-3039	3,750 psi (25.8 MPa)	3,000 psi (20.7 MPa)
Laminate Thickness		0.05 in. (1.3 mm)	0.05 in. (1.3mm)

* Gross laminate design properties based on ACI 440 suggested guidelines will vary slightly. Contact Fyfe Co. LLC engineers to confirm project specification values and design methodology.

COVERAGE
Approximately 675 sq. ft. surface area with 3 to 4 units of Tyfo® S Epoxy and 1 roll of Tyfo® SEH-51A Fabric when used with the Tyfo® Saturator.

PACKAGING
Order Tyfo® S Epoxy in 55-gallon (208L) drums or pre-measured units in 5-gallon (19L) containers. Order Tyfo® SEH-51A Fabric in 54" x 150 lineal foot (1.4m x 45.7m) rolls. Typically ships in 12" x 13" x 64" (305mm x 330mm x 1626mm) boxes.

EPOXY MIX RATIO
100.0 component A to 42.0 component B by volume. (100 component A to 34.5 component B by weight.)

SHELF LIFE
Epoxy - two years in original, unopened and properly stored containers.
Fabric - ten years in proper storage conditions.

STORAGE CONDITIONS
Store at 40° to 90° F (4° to 32° C). Avoid freezing. Store rolls flat, not on ends, at temperatures below 100° F (38° C). Avoid moisture and water contamination.

CERTIFICATE OF COMPLIANCE
- Will be supplied upon request, complete with state and federal packaging laws with copy of labels used.
- Material safety data sheets will be supplied upon request.
- Possesses 0% V.O.C. level.

10/07 Tyfo® SEH-51A

EPOXY MATERIAL PROPERTIES

Curing Schedule 72 hours post cure at 140° F (60° C).

PROPERTY	ASTM METHOD	TYPICAL TEST VALUE*
T_g	ASTM D-4065	180° F (82° C)
Tensile Strength[1], psi	ASTM D-638 Type 1	10,500 psi (72.4 MPa)
Tensile Modulus, psi	ASTM D-638 Type 1	461,000 psi (3.18 GPa)
Elongation Percent	ASTM D-638 Type 1	5.0%
Flexural Strength, psi	ASTM D-790	17,900 psi (123.4 MPa)
Flexural Modulus, psi	ASTM D-790	452,000 psi (3.12 GPa)

[1] Testing temperature: 70° F (21° C)   Crosshead speed: 0.5 in. (13mm)/min.   Grips Instron 2716-0055 - 30 kips
* Specification values can be provided upon request.

Figure A.1 - Fibreglass Cloth [reproduced from Fyfe Co., 2008]

HOW TO USE THE TYFO® S COMPOSITE SYSTEM

DESIGN
The Tyfo® System shall be designed to meet specific design criteria. The criteria for each project is dictated by the engineer of record and any relevant building codes and/or guidelines. The design should be based on the allowable strain for each type of application and the design modulus of the material. The Fyfe Co. LLC engineering staff will provide preliminary design at no obligation.

INSTALLATION
Tyfo® System to be installed by Fyfe Co. LLC trained and certified applicators. Installation shall be in strict compliance with the Fyfe Co. LLC Quality Control Manual.

SURFACE PREPARATION
The required surface preparation is largely dependent on the type of element being strengthened. In general, the surface must be clean, dry and free of protrusions or cavities, which may cause voids behind the Tyfo® composite. Column surfaces that will receive continuous wraps typically require only a broom cleaning. Discontinuous wrapping surfaces (walls, beams, slabs, etc.) typically require a light sandblast, grinding or other approved methods to prepare for bonding. Tyfo® Fibrwrap® Anchors are incorporated in some designs. The Fyfe Co. LLC engineering staff will provide the proper specifications and details based on the project requirements.

LIMITATIONS
Minimum application temperature of the epoxy is 40° F (4° C). DO NOT THIN, solvents will prevent proper cure.

CAUTION!

COMPONENT A - Irritant:
Prolonged contact to the skin may cause irritation. Avoid eye contact.

COMPONENT B - Irritant:
Contact with skin may cause severe burns. Avoid eye contact. Product is a strong sensitizer. Use of safety goggles and chemical resistant gloves recommended. Remove contaminated clothing. Avoid breathing vapors. Use adequate ventilation. Use of an organic vapor respirator recommended.

SAFETY PRECAUTIONS
Use of an approved particle mask is recommended for possible airborne particles. Gloves are recommended when handling fabrics to avoid skin irritation. Safety glasses are recommended to prevent eye irritation.

FIRST AID
In case of skin contact, wash thoroughly with soap and water. For eye contact, flush immediately. For respiratory problems, remove to fresh air. Wash clothing before reuse.

TYFO® S COMPOSITE SAMPLES
Please note that field samples are to be cured for 48-hours at 140°F (60°C) before testing. Testing shall be in accordance with ASTM D-3039 and Fyfe Co. LLC sample preparation and testing procedures.

SHIPPING LABELS CONTAIN
- State specification number with modifications, if applicable
- Component designation
- Type, if applicable
- Manufacturer's name
- Date of manufacture
- Batch name
- State lot number, if applicable
- Directions for use
- Warnings or precautions by law

KEEP CONTAINER TIGHTLY CLOSED.
NOT FOR INTERNAL CONSUMPTION.
CONSULT MATERIAL SAFETY DATA SHEET (MSDS) FOR MORE INFORMATION.
KEEP OUT OF REACH OF CHILDREN.
FOR INDUSTRIAL USE ONLY.

MIXING
For pre-measured units in 5-gallon (19L) containers, pour the contents of component B into the pail of component A. For drums, premix each component: 100.0 parts of component A to 42.0 parts of component B by volume (100 parts of component A to 34.5 parts of component B by weight). Mix thoroughly for five minutes with a Tyfo® low speed mixer at 400-600 RPM until uniformly blended.

APPLICATION
Feed fabric through the Tyfo® Saturator and apply using the Tyfo® wrapping equipment or approved hand methods. See data sheet on this equipment. Hand saturation is allowable, provided the epoxy is applied uniformly and meets the specifications.

CLEANUP
Collect with absorbent material, flush with water. Dispose of in accordance with local disposal regulations. Uncured material can be removed with approved solvent. Cured materials can only be removed mechanically.

Fyfe Co. LLC
Tyfo® Fibrwrap® Systems
Nancy Ridge Technology Center
6310 Nancy Ridge Drive, Suite 103, San Diego, CA 92121
Tel: 858.642.0694 Fax: 858.642.0947
E-mail: info@fyfeco.com Web: http://www.fyfeco.com

Figure A.1 (continued) - Fibreglass Cloth [reproduced from Fyfe Co., 2008]

FYFE Co. LLC
Tyfo® Fibrwrap® Systems

Tyfo® S
Saturant Epoxy

DESCRIPTION
The Tyfo® S Epoxy is a two-component epoxy matrix material for bonding applications. The Tyfo® S Epoxy combined with Tyfo SEH and Tyfo SCH fabrics is a NSF/ANSI Standard 61 listed product for drinking water systems. It is a high elongation material which gives optimum properties as a matrix for the Tyfo® Fibrwrap System. It provides a long working time for application, with no offensive odor. Tyfo® S Epoxy may also be thickened and used as a prime or finish coat depending upon the project requirements.

USE
The Tyfo® S Epoxy matrix material is combined with the Tyfo® fabrics to provide a wet-layup composite system for strengthening structural members.

ADVANTAGES
- ICC-ES ESR-2103 listed product
- NSF/ANSI Standard 61 listed product for drinking water systems
- Good high temperature properties
- Good low temperature properties
- Long working time
- High elongation
- Ambient cure
- 100% solvent-free

HOW TO USE THE TYFO® S EPOXY

INSTALLATION
Tyfo® System to be installed by Fyfe Co. LLC trained and certified applicators. Installation shall be in strict compliance with the Fyfe Co. LLC Quality Control Manual.

SURFACE PREPARATION
The required surface preparation is largely dependent on the type of element being strengthened. In general, the surface must be clean, dry and free of protrusions or cavities, which may cause voids behind the Tyfo® composite. Column surfaces that will receive continuous wraps typically require only a broom cleaning. Discontinuous wrapping surfaces (walls, beams, slabs, etc.) typically require a light sandblast, grinding or other approved methods to prepare for bonding. Mechanical anchors are incorporated in some designs. The Fyfe Co. LLC engineering staff will provide the proper specifications and details based on the project requirements.

MIXING
For pre-measured units in 5-gallon containers, pour the contents of component B into the pail of component A. For drums, premix each component: 100.0 parts of component A to 42.0 parts of component B by volume (100 parts of component A to 34.5 parts of component B by weight). If material is too thick, drum heaters may be used on metal containers, or heat unmixed components by placing containers in 130° F (54° C) tap water or sunlight, if available, until the desired viscosity is achieved. Do not thin; solvents will prevent proper cure. Mix thoroughly for five minutes with a low speed mixer at 400-600 RPM until uniformly blended. When using as a prime coat or finish coat, Tyfo® S Epoxy may be thickened in the field to the desired consistency.

APPLICATION
Tyfo® S Epoxy is applied to a variety of Tyfo® fabrics using the Tyfo® Saturator or by approved hand-applied methods. See data sheet on this equipment. Hand saturation is allowable, provided the epoxy is applied uniformly and meets the specifications. Tyfo® S Epoxy can also be applied as a prime coat by brush or roller.

LIMITATIONS
Minimum application temperature of the epoxy is 40° F (4° C). DO NOT THIN; solvents will prevent proper cure.

COVERAGE
Approximately 0.8 pounds of epoxy per 1.0 pound of fabric when our Tyfo® Saturator is used. When used as a prime coat the coverage is highly dependent upon the existing surface.

PACKAGING
Order in 55-gallon drums or pre-measured units in 5-gallon containers.

MIX RATIO
100.0 parts of component A to 42.0 parts of component B by volume. (100 parts of component A to 34.5 parts of component B by weight).

SHELF LIFE
Two years in original, unopened and properly stored containers.

STORAGE CONDITIONS
Store at 40° to 90° F (4° to 32° C). Avoid freezing.

CERTIFICATE OF COMPLIANCE
- Will be supplied upon request, complete with state and federal packaging laws with copy of labels used.
- Material safety data sheets will be supplied upon request.
- Possesses 0% V.O.C. level, per ASTM D-2369.

1/08 Tyfo® S

EPOXY COMPONENT PROPERTIES	
Color	Component A is clear to pale yellow Component B is clear
Viscosity	Component A at 77° F (25° C) is 11,000-13,000 cps ASTM D-2392-80 Component B at 77° F (25° C) is 11 cps ASTM D-2393-80
Pot Life	3 to 6 hours at 68° F (20° C)
Viscosity of Mixed Product	600-700 cps
Density at 68° F (20° C) (Pound/Gallon)	Component A = 9.7 (4.4kg/3.79L) Component B = 7.9 (3.6kg/3.79L) Mixed product = 9.17 (4.2kg/3.79L)

Figure A.2 - Epoxy [reproduced from Fyfe Co., 2008]

EPOXY MATERIAL PROPERTIES		
Curing Schedule 72 hours post cure at 140° F (60° C).		
PROPERTY	ASTM METHOD	TYPICAL TEST VALUE[2]
T_g	ASTM D-4065	180°F (82°C)
Tensile Strength[1], minimum psi	ASTM D-638 Type 1	7,250 psi (50.0 MPa)
Tensile Modulus, psi	ASTM D-638 Type 1	461,000 psi (3.18 GPa)
Elongation Percent	ASTM D-638 Type 1	5.0%
Flexural Strength, psi	ASTM D-790	17,900 psi (123.4 MPa)
Flexural Modulus, psi	ASTM D-790	452,000 psi (3.12 GPa)

[1] Testing temperature: 70° F (21° C) Crosshead speed: 0.5 in. (13mm)/min. Grips Instron 2716-0055 - 30 kips
[2] Specification values can be provided upon request.

SHIPPING LABELS CONTAIN

- State specification number with modifications, if applicable
- Component designation
- Type, if applicable
- Manufacturer's name
- Date of manufacture
- Batch name
- State lot number, if applicable
- Directions for use
- Warnings or precautions required by law

KEEP CONTAINER TIGHTLY CLOSED.
NOT FOR INTERNAL CONSUMPTION.
CONSULT MATERIAL SAFETY DATA SHEET (MSDS) FOR MORE INFORMATION.
KEEP OUT OF REACH OF CHILDREN.
FOR INDUSTRIAL USE ONLY.

CAUTION!

COMPONENT A - Irritant:
Prolonged contact to the skin may cause irritation. Avoid eye contact.

COMPONENT B - Irritant:
Contact with skin may cause severe burns. Avoid eye contact. Product is a strong sensitizer. Use of safety goggles and chemical resistant gloves recommended. Remove contaminated clothing. Avoid breathing vapors. Use adequate ventilation. Use of an organic vapor respirator recommended.

FIRST AID

In case of skin contact, wash thoroughly with soap and water. For eye contact, flush immediately with plenty of water; contact physician immediately. For respiratory problems, remove to fresh air. Wash clothing before reuse.

CLEANUP

Collect with absorbent material, flush with water. Dispose of in accordance with local disposal regulations. Uncured material can be removed with approved solvent. Cured materials can only be removed mechanically.

Fyfe Co. LLC
Tyfo® Fibrwrap® Systems
Nancy Ridge Technology Center
6310 Nancy Ridge Drive, Suite 103, San Diego, CA 92121
Tel: 858.642.0694 Fax: 858.642.0947
E-mail: info@fyfeco.com Web: http://www.fyfeco.com

Figure A.2 (continued) - Epoxy [reproduced from Fyfe Co., 2008]

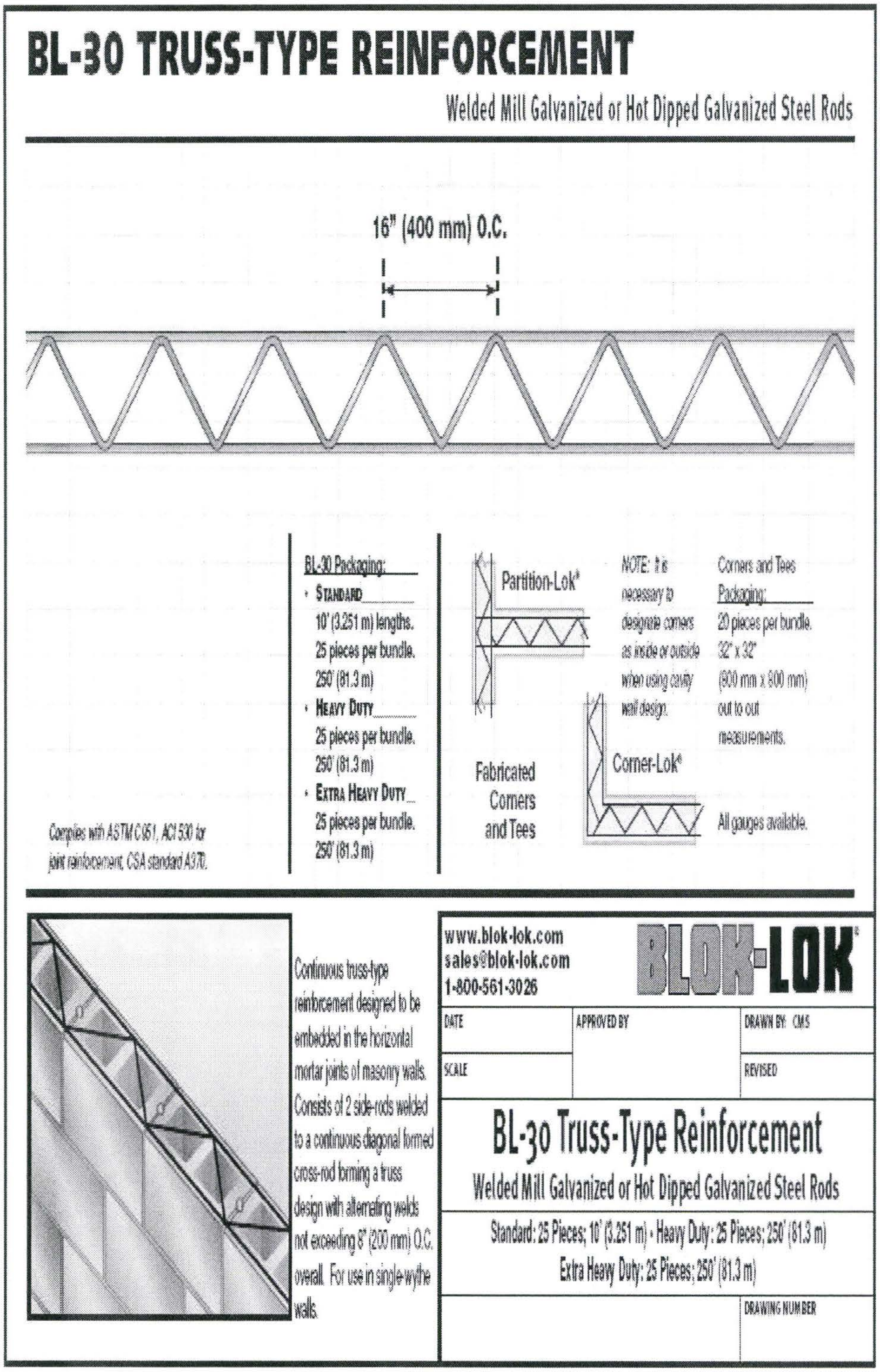

Figure A.3 - Truss Type Joint Reinforcement [reproduced from BLOK-LOK Ltd., 2007]

Joint Reinforcement

Joint reinforcement is installed in horizontal mortar joints of masonry for shrinkage stress control. For joint reinforcement to effectively distribute stress it must be adequately bonded through the mortar so that the masonry and reinforcement act together.

Table A, shown below, shows wire size and properties for steel joint reinforcement material.

Table A
Wire Sizes and Properties for Steel Joint Reinforcement

Continuous System Designation	Longitudinal Wires	Cross or Diagonal Wire
Standard	0.144" (9 ga) (3.66 mm)	0.144" (9 ga) (3.66 mm)
Heavy Duty	0.1875" (3/16") (4.76 mm)	0.144" (9 ga) (3.66 mm)
Extra Heavy Duty	0.1875" (3/16") (4.76 mm)	3/16" (4.76 mm)

ASTM A82 and CSA G30-3 Wire Requirements (for cold drawn steel wire).

Tensile Strength: 80,000 psi
Yield Strength: 70,000 psi
Reduction of Area: 30%

	9 Gauge Wire	3/16 Wire
Wire Diameter	0.144 in. (3.66 mm)	0.1875 in. (4.76 mm)
Cross-Sectional	10.52 sq. mm	17.80 sq. mm
Area Per Wire	(.0163 sq. in.)	(.0276 sq. in.)
Yield Load	1140 lbs. (5075 N)	[illegible] lbs. ([illegible] N)
Ultimate Load	1303 lbs. (5800 N)	2210 lbs. ([illegible] N)

Finishes

Blok-Lok continuous reinforcement systems are available in a variety of finishes.

Table B
Finishes for Joint Reinforcement Systems

Finish	Material	Specification	Coating Specification	Minimum Coating Mass
Mill Galvanized	Wire	CSA A370-04	A641	.010"
Hot Dipped Galvanized After Fabrication *	Wire	CSA A370-04	ASTM A153 Class B2	1.65 oz/ft² (457 g/m²)
Stainless Steel	Wire	ASTM 79 - AISI Type 302 & 304	None	Uncoated
Hot Dipped Galvanized	Sheet 3.18 mm			

* [illegible]

Stress Distribution

Continuous joint reinforcement is used to distribute stress concentrations that occur above and below windows, or where wall sections are reduced because of embedded columns, and below concentrated loads such as beams and slabs. An important application of stress distribution joint reinforcement is to safeguard the integrity of masonry walls to such unexpected and difficult-to-design-for events as industrial explosions and accidents.

www.blok-lok.com
sales@blok-lok.com
1-800-561-3026

BLOK-LOK

Figure A.3 (continued) - Truss Type Joint Reinforcement [reproduced from BLOK-LOK Ltd., 2007]

Table A.1 – Mortar compressive strengths

Batch#	Cube#	Failure Load(kN)	Strength(Mpa)
1	1	47.8	18.4
	1	48.5	18.7
	1	43.5	16.7
2	2	59.5	22.9
	2	50.0	19.2
	2	56.5	21.7
3	3	50.5	19.4
	3	52.5	20.2
	3	55.5	21.3
1A	1A	53.5	20.6
	1A	58.5	22.5
	1A	54.0	20.8
2A	2A	50.0	19.2
	2A	38.0	14.6
	2A	61.5	23.7
3A	3A	61.5	23.7
	3A	61.5	23.7
	3A	60.0	23.1
1B	1B	72.0	27.7
	1B	72.0	27.7
	1B	75.5	29.0
2B	2B	71.0	27.3
	2B	62.0	23.8
	2B	64.0	24.6
3B	3B	49.0	18.8
	3B	57.0	21.9
	3B	58.0	22.3
1C	1C	65.5	25.2
	1C	61.0	23.5
	1C	59.5	22.9
2C	2C	54.0	20.8
	2C	51.0	19.6
	2C	56.5	21.7
3C	3C	61.5	23.7
	3C	55.0	21.2
	3C	58.5	22.5
1D	1D	62.0	23.8
	1D	64.5	24.8
	1D	60.5	23.3

AVG.	**57.8**	**22.2**
	C.O.V. (%) =	**9.1**

APPENDIX B: RAW EXPERIMENTAL DATA

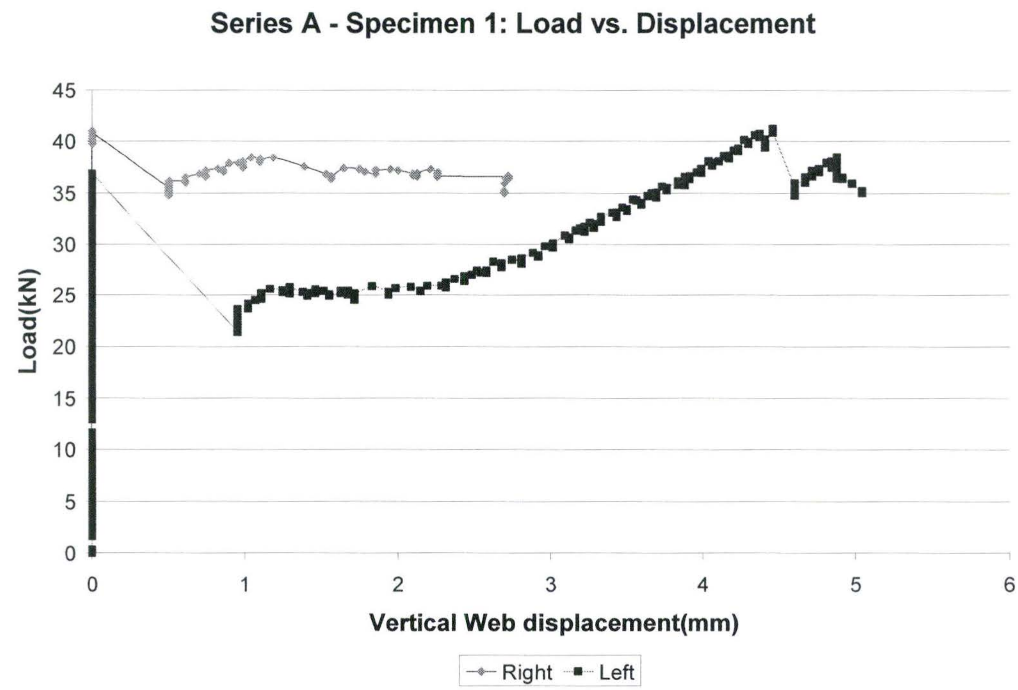

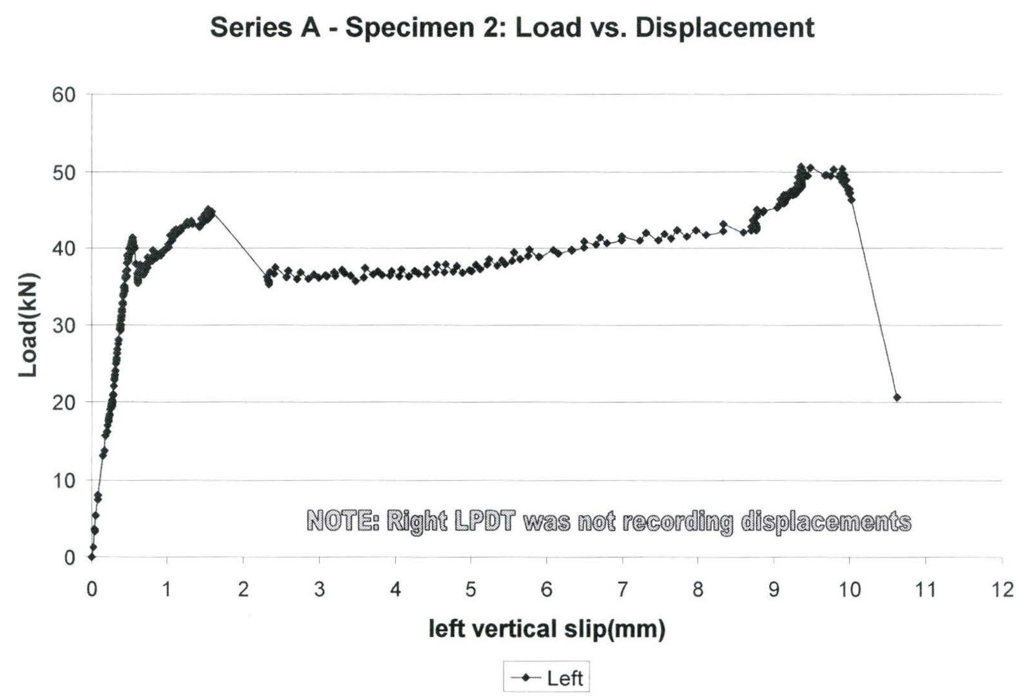

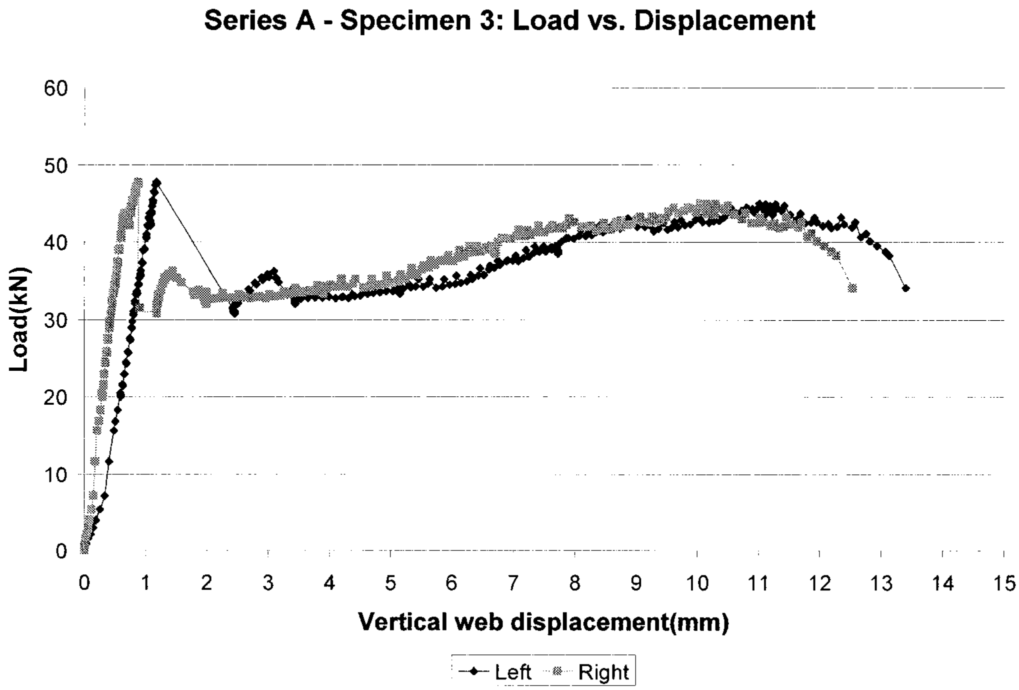

Series A - Specimen 3: Load vs. Displacement
Load(kN)
60
50
40
30
20
10
0
0 1 2 3 4 5 6 7 8 9 10 11 12 13 14 15
Vertical web displacement(mm)
Left
Right

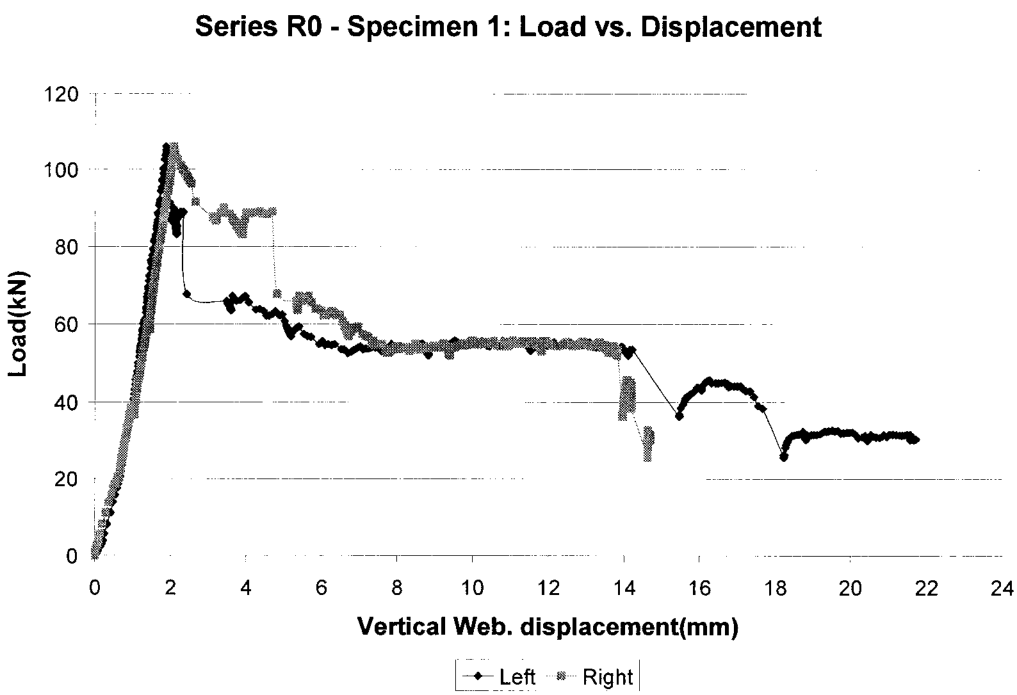

Series R0 - Specimen 1: Load vs. Displacement
Load(kN)
120
100
80
60
40
20
0
0 2 4 6 8 10 12 14 16 18 20 22 24
Vertical Web. displacement(mm)
Left
Right

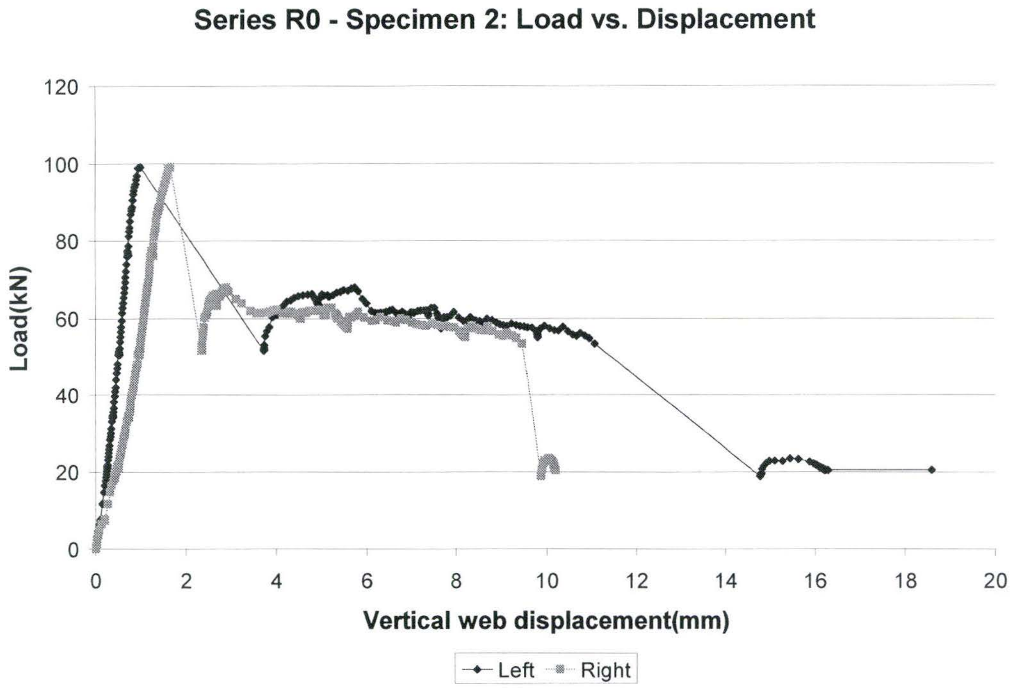
Series R0 - Specimen 2: Load vs. Displacement
Load(kN)
0
20
40
60
80
100
120
0
2
4
6
8
10
12
14
16
18
20
Vertical web displacement(mm)
Left
Right

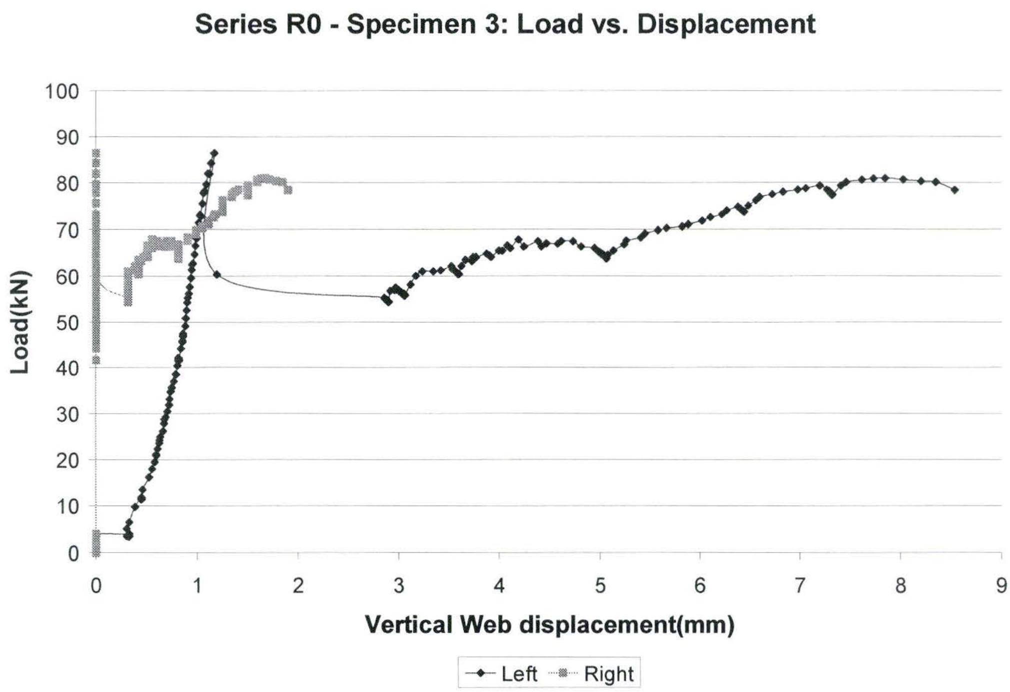
Series R0 - Specimen 3: Load vs. Displacement
Load(kN)
0
10
20
30
40
50
60
70
80
90
100
0
1
2
3
4
5
6
7
8
9
Vertical Web displacement(mm)
Left
Right

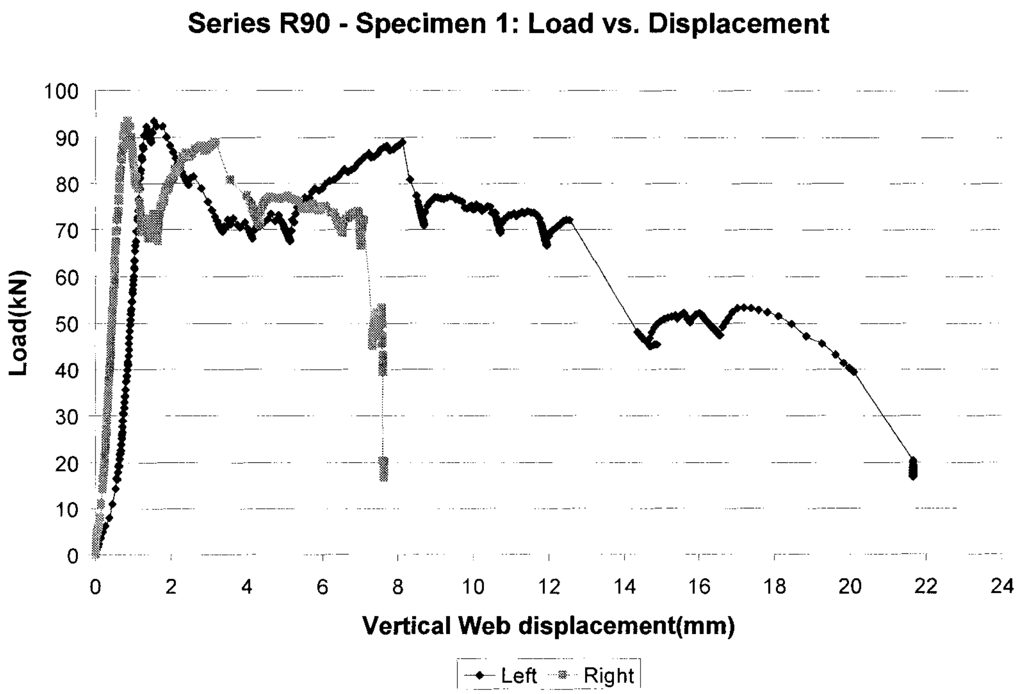
Series R90 - Specimen 1: Load vs. Displacement
Load(kN)
0
10
20
30
40
50
60
70
80
90
100
0
2
4
6
8
10
12
14
16
18
20
22
24
Vertical Web displacement(mm)
Left
Right

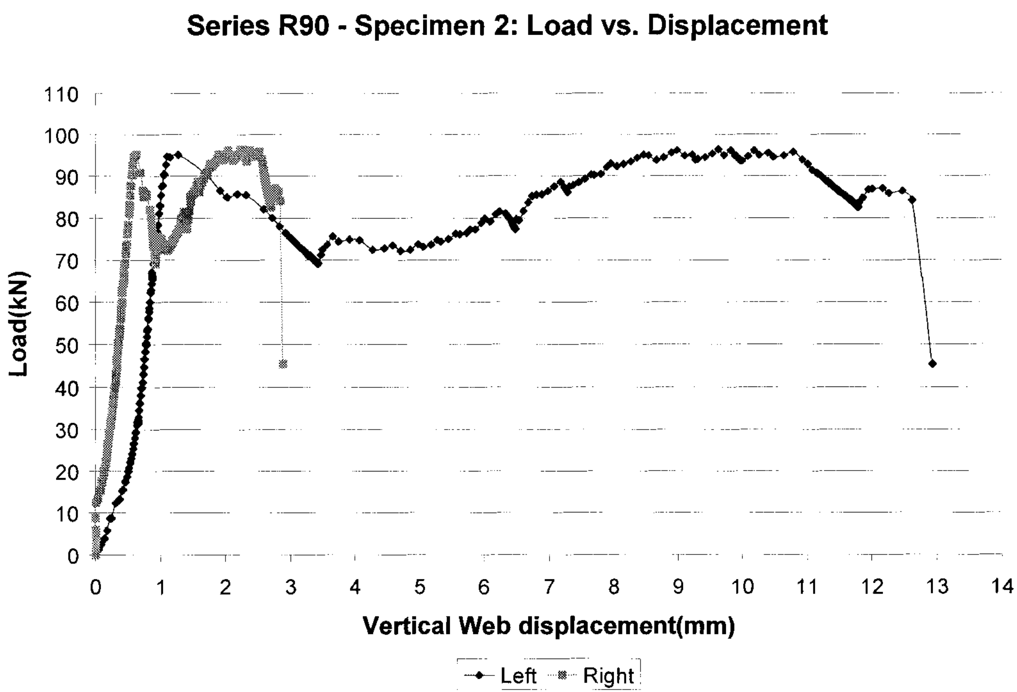
Series R90 - Specimen 2: Load vs. Displacement
Load(kN)
0
10
20
30
40
50
60
70
80
90
100
110
0
1
2
3
4
5
6
7
8
9
10
11
12
13
14
Vertical Web displacement(mm)
Left
Right

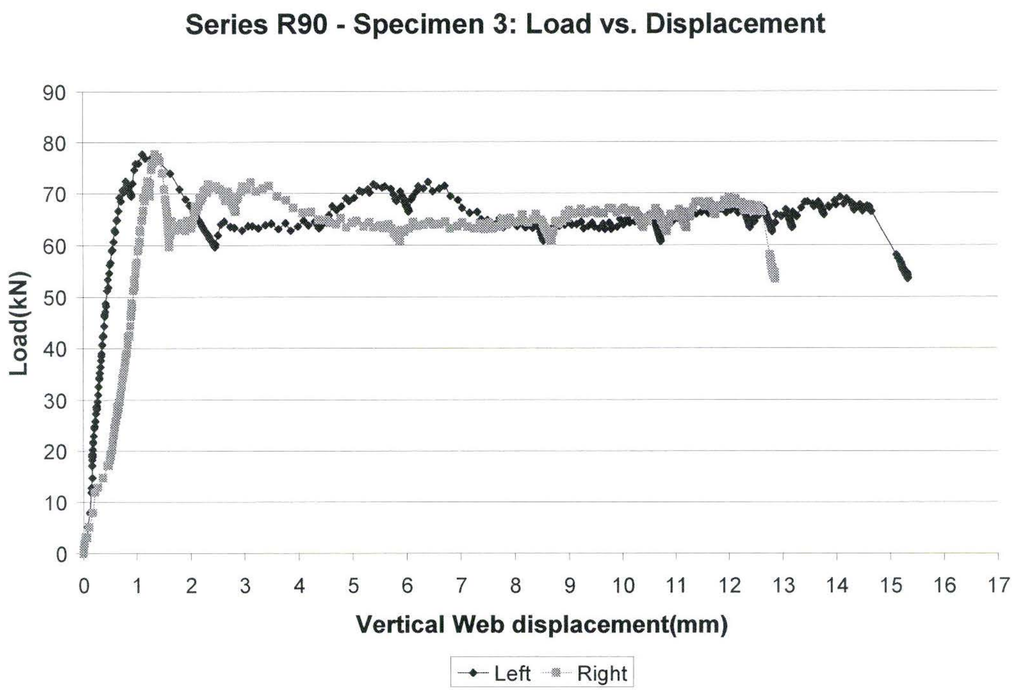
Series R90 - Specimen 3: Load vs. Displacement
Load(kN)
Vertical Web displacement(mm)
Left
Right

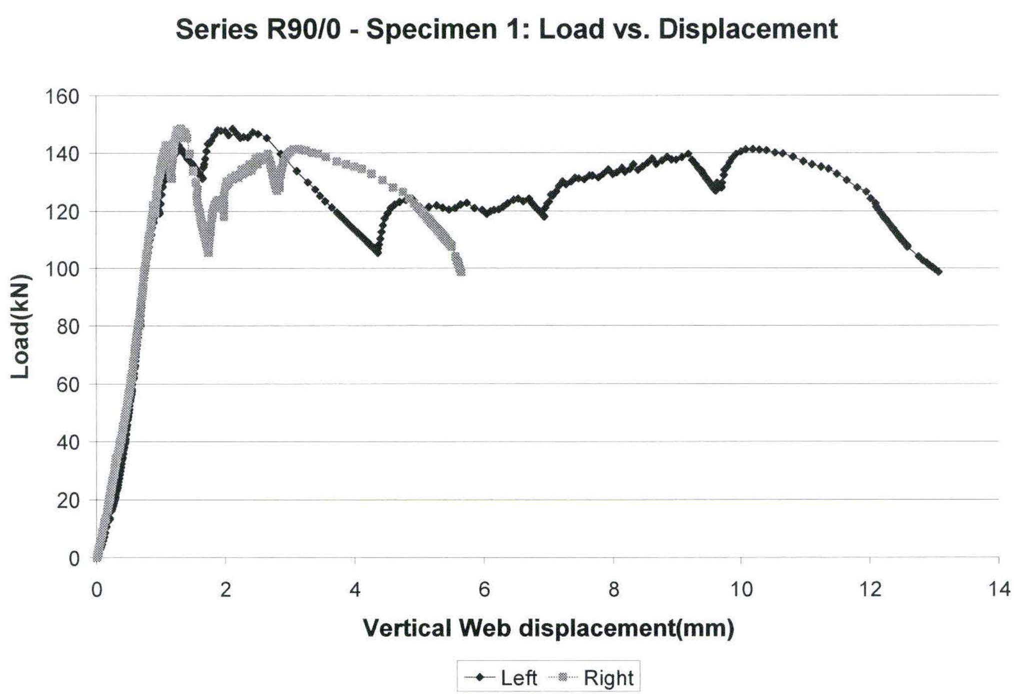
Series R90/0 - Specimen 1: Load vs. Displacement
Load(kN)
Vertical Web displacement(mm)
Left
Right

Series R90/0 - Specimen 2: Load vs. Displacement

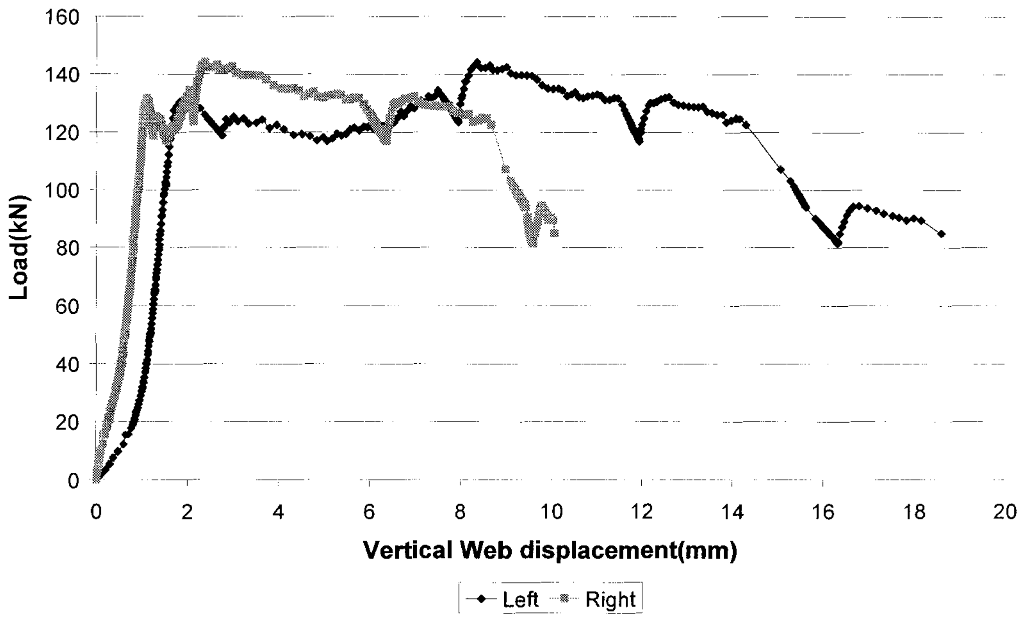

Series R90/0 - Specimen 3: Load vs. Displacement

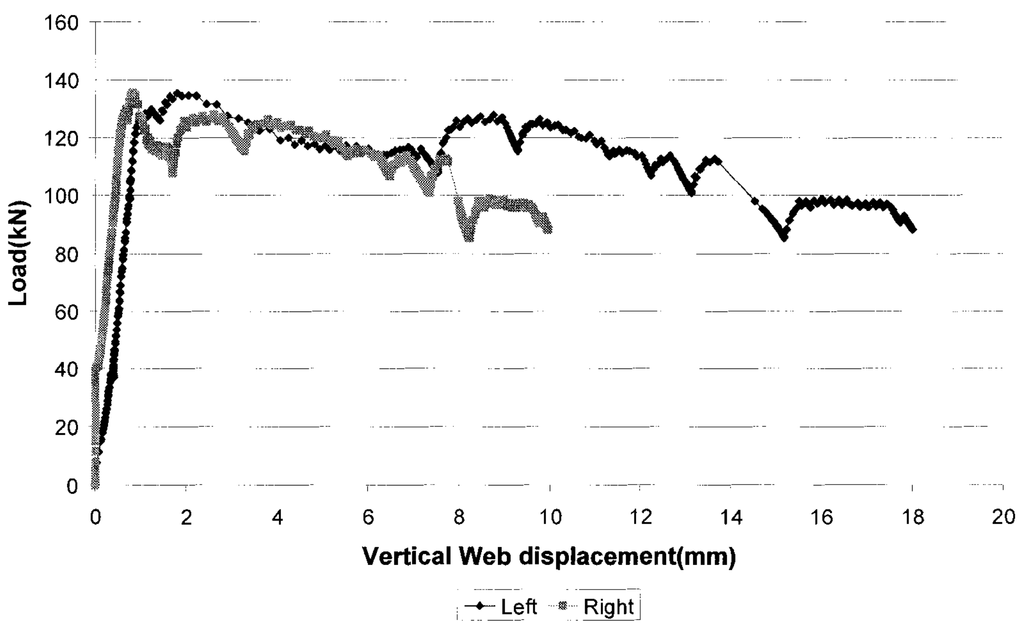

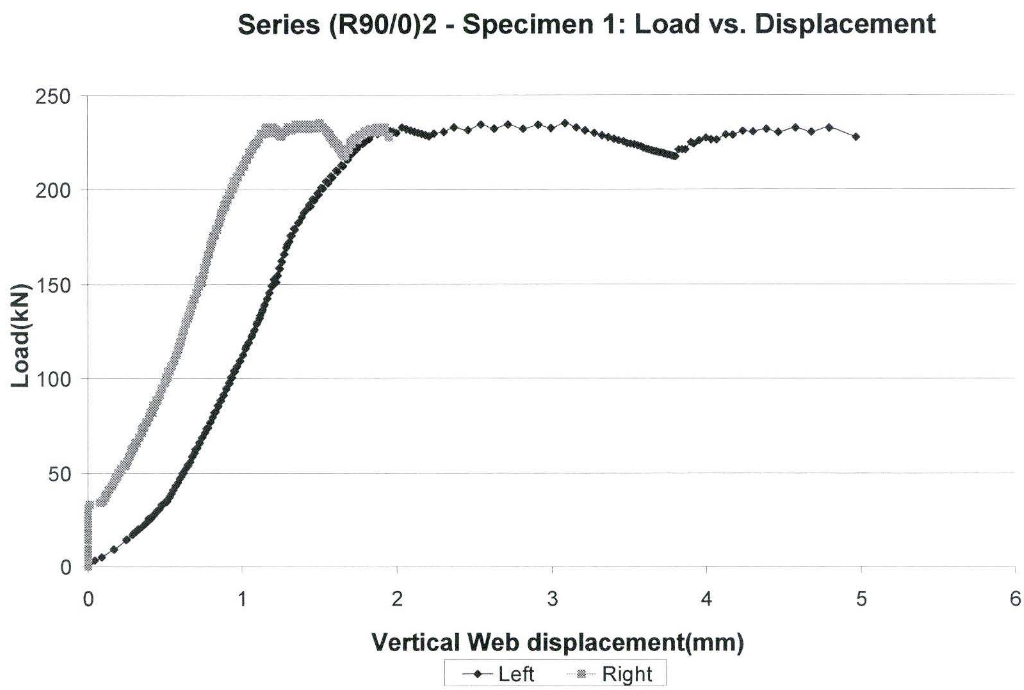
Series (R90/0)2 - Specimen 1: Load vs. Displacement
250
200
150
100
50
0
Load(kN)
0
1
2
3
4
5
6
Vertical Web displacement(mm)
Left
Right

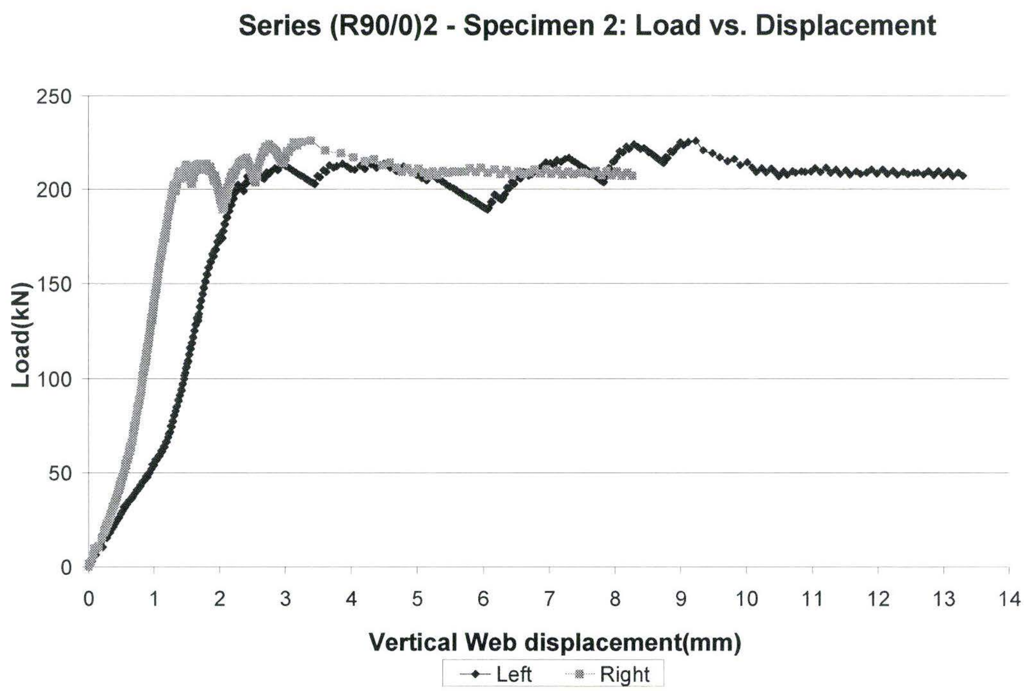
Series (R90/0)2 - Specimen 2: Load vs. Displacement
250
200
150
100
50
0
Load(kN)
0
1
2
3
4
5
6
7
8
9
10
11
12
13
14
Vertical Web displacement(mm)
Left
Right

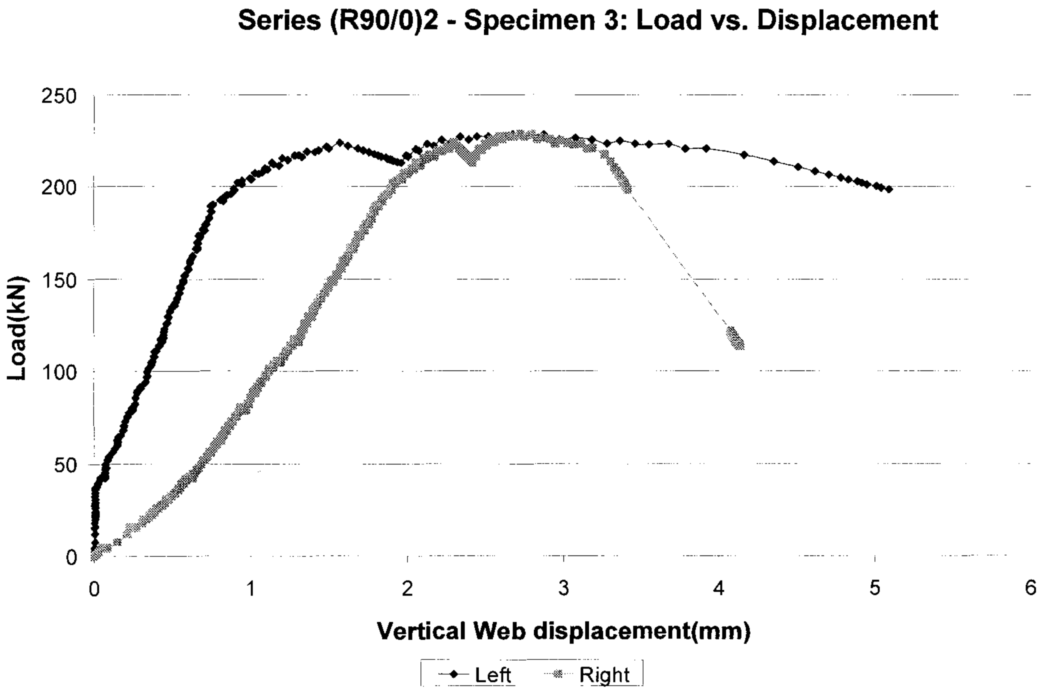
Series (R90/0)2 - Specimen 3: Load vs. Displacement
250
200
150
100
50
0
Load(kN)
0
1
2
3
4
5
6
Vertical Web displacement(mm)
Left
Right

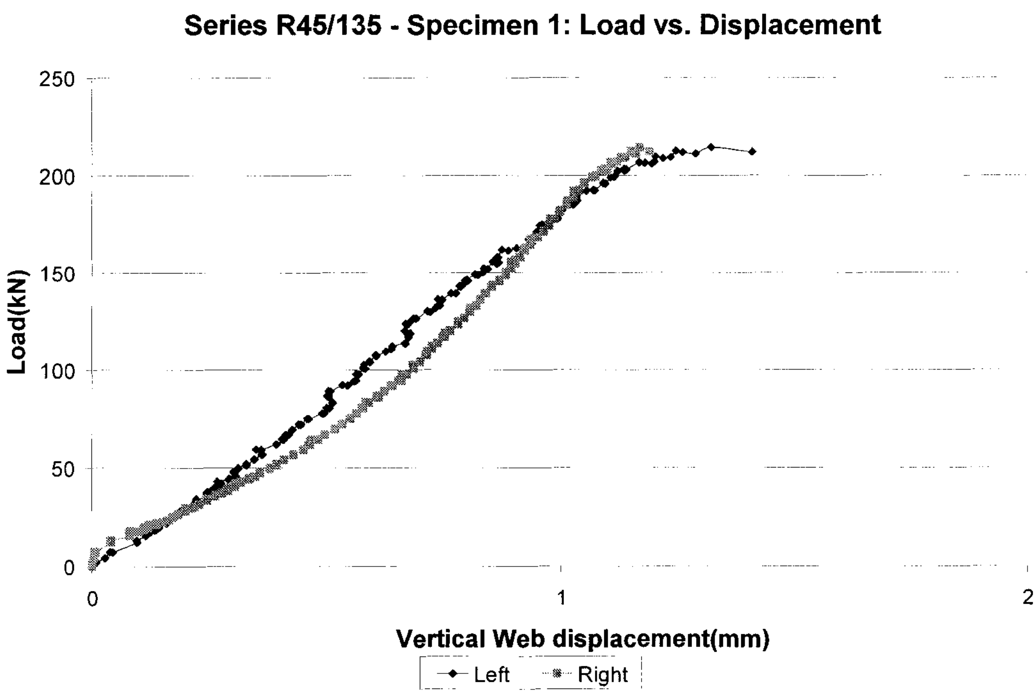
Series R45/135 - Specimen 1: Load vs. Displacement
250
200
150
100
50
0
Load(kN)
0
1
2
Vertical Web displacement(mm)
Left
Right

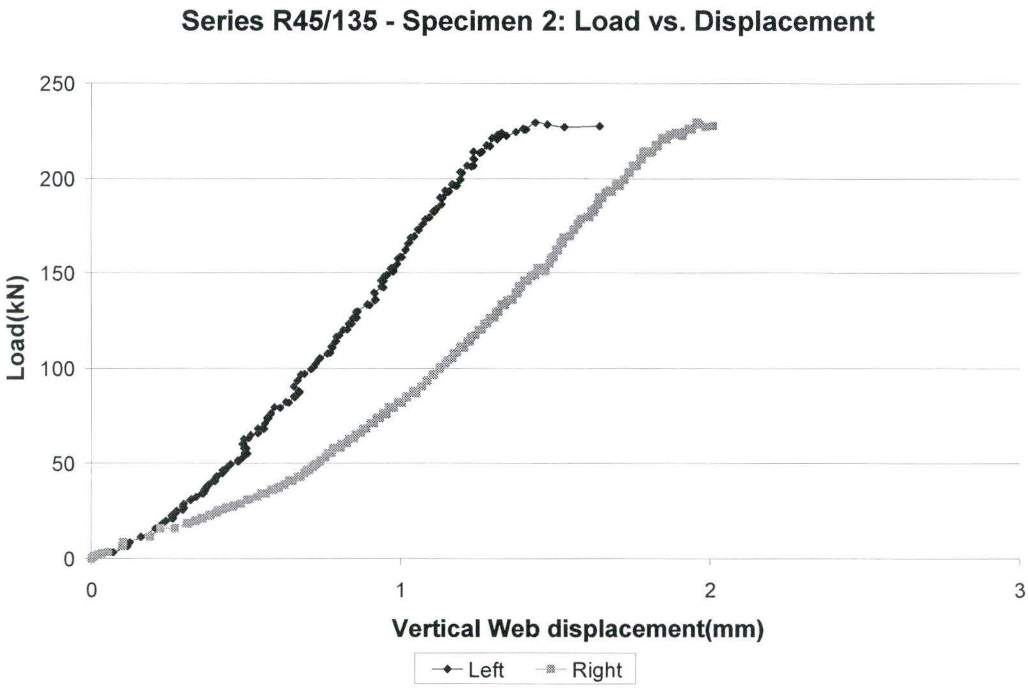
Series R45/135 - Specimen 2: Load vs. Displacement
250
200
150
100
50
0
Load(kN)
0
1
2
3
Vertical Web displacement(mm)
Left
Right

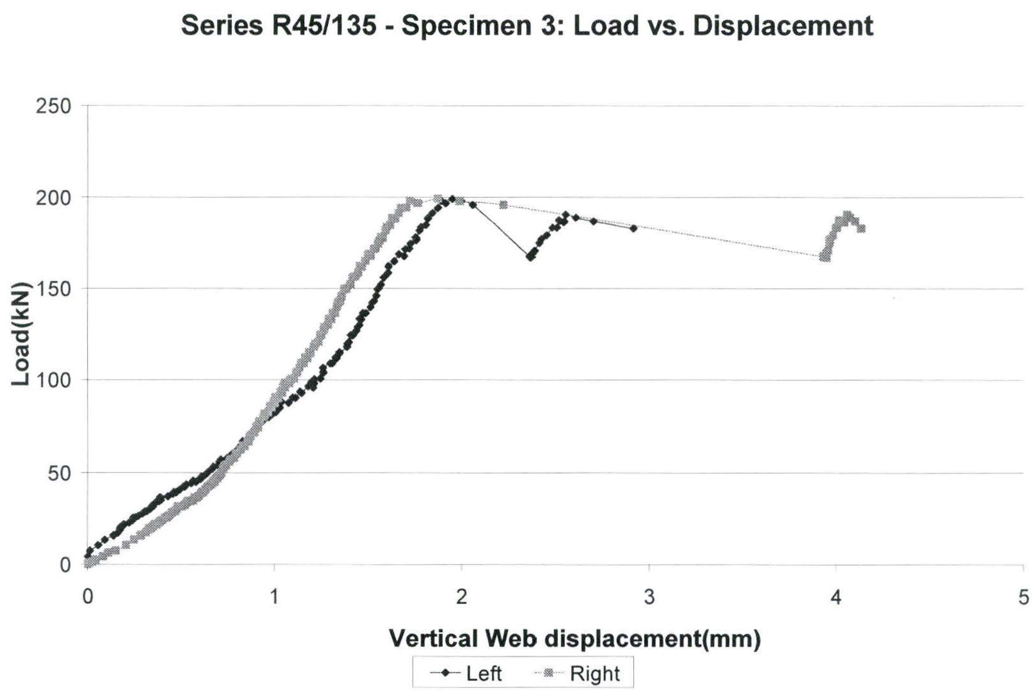
Series R45/135 - Specimen 3: Load vs. Displacement
250
200
150
100
50
0
Load(kN)
0
1
2
3
4
5
Vertical Web displacement(mm)
Left
Right

Series **A** – Specimen 1: Test Results

Load (kN)	Vertical Slip between Flange and Web(mm)*		Horizontal Separation between Flange and Web(mm)*		Remarks
	Left side(#1)	Right side(#2)	Left side(#3)	Right side(#4)	
0	0.00	0.00	0.00	0.00	
10	0.00	0.00	0.00	0.00	
20	0.00	0.00	0.04	0.01	
30	0.00	0.00	0.07	0.05	
37	0.01	0.00	0.07	0.15	Ultimate Load **
22	0.95	0.00	0.06	0.32	Web slipping *** (Left side)
41	4.46	0.00	0.15	0.16	Testing terminated **** (Snapping noise of steel ties)

* Downward vertical displacements are positive and outward horizontal separations are positive

** Vertical mortar joint cracked through on left side

*** Further loading after failure

**** Post-slip failure load higher than cracking load

Series **A** – Specimen 2: Test Results

Load (kN)	Vertical Slip between Flange and Web(mm)*		Horizontal Separation between Flange and Web(mm)*		Remarks
	Left side(#1)	Right side(#2)	Left side(#3)	Right side(#4)	
0	0.00	0.00	0.00	0.00	
8	0.08	0.00	0.00	0.00	
20	0.27	0.00	0.00	0.00	
30	0.39	0.00	0.00	0.00	
45	1.58	0.00	0.00	0.12	Ultimate Load **
36	2.31	0.00	0.00	0.26	Web slipping *** (Left side)
51	9.36	0.00	0.00	0.35	Testing terminated **** (Snapping noise of steel ties)

* Downward vertical displacements are positive and outward horizontal separations are positive

** Vertical mortar joint cracked through on left side

*** Further loading after failure

**** Post-slip failure load higher than cracking load

Series **A** – Specimen 3: Test Results

Load (kN)	Vertical Slip between Flange and Web(mm)*		Horizontal Separation between Flange and Web(mm)*		Remarks
	Left side(#1)	Right side(#2)	Left side(#3)	Right side(#4)	
0	0.00	0.00	0.00	0.00	
12	0.40	0.18	0.00	0.01	
20	0.59	0.29	0.00	0.02	
31	0.8	0.44	0.01	0.04	
40	1.00	0.59	0.08	0.06	
48	1.17	0.87	0.17	0.08	Ultimate Load **
32	2.41	0.90	0.46	0.09	Web slipping *** (Left side & Right side)
45	11.0	10.04	1.12	0.10	Testing terminated **** (Snapping noise of steel ties)

* Downward vertical displacements are positive and outward horizontal separations are positive

** Vertical mortar joint cracked through on left side and right side

*** Further loading after failure

**** Local spalling of concrete block on left flange observed in proximity of reinforcement.

Series **R0°** – Specimen 1: Test Results

Load (kN)	Vertical Slip between Flange and Web(mm)*		Horizontal Separation between Flange and Web(mm)*		Remarks
	Left side(#1)	Right side(#2)	Left side(#3)	Right side(#4)	
0	0.00	0.00	0.00	0.00	
20	0.63	0.60	0.00	0.00	
41	1.02	1.06	0.00	0.00	
59	1.31	1.45	0.01	0.00	
79	1.53	1.69	0.06	0.02	
100	1.79	2	0.08	0.06	
106	1.85	2.07	0.08	0.08	Ultimate Load **
53	6.69	7.74	0.69	0.80	Web slipping *** (Left side & Right side)
53	14.20	13.82	1.14	1.44	Testing terminated (Snapping noise of steel ties)

* Downward vertical displacements are positive and outward horizontal separations are positive

** Initiation of vertical rupture of GFRP Laminate

*** Further loading after failure

Series **R0°** – Specimen 2: Test Results

Load (kN)	Vertical Slip between Flange and Web(mm)*		Horizontal Separation between Flange and Web(mm)*		Remarks
	Left side(#1)	Right side(#2)	Left side(#3)	Right side(#4)	
0	0.00	0.00	0.00	0.00	
20	0.24	0.45	0.00	0.00	
41	0.43	0.82	0.00	0.00	
59	0.57	1.06	0.00	0.02	
79	0.73	1.28	0.00	0.05	
99	1.00	1.66	0.00	0.12	Ultimate Load **
51	3.73	2.35	0.00	0.13	Web slipping *** (Left side & Right side)
68	5.73	2.89	0.00	0.13	
53	11.07	9.46	0.00	0.30	Testing terminated (Snapping noise of steel ties)

* Downward vertical displacements are positive and outward horizontal separations are positive

** Initiation of vertical rupture of GFRP Laminate

*** Further loading after failure

Series **R0°** – Specimen 3: Test Results

Load (kN)	Vertical Slip between Flange and Web(mm)*		Horizontal Separation between Flange and Web(mm)*		Remarks
	Left side(#1)	Right side(#2)	Left side(#3)	Right side(#4)	
0	0.00	0.00	0.00	0.00	
19	0.58	0.00	0.00	0.00	
40	0.80	0.00	0.00	0.00	
60	0.94	0.00	0.00	0.00	
80	1.09	0.00	0.56	0.00	
86	1.17	0.00	0.61	0.01	Ultimate Load **
60	1.19	0.00	0.73	0.01	
55	2.88	0.32	1.13	0.03	Web slipping *** (Left side & Right side)
81	7.85	1.68	1.01	0.08	Testing terminated (Snapping noise of steel ties)

* Downward vertical displacements are positive and outward horizontal separations are positive

** Initiation of vertical rupture of GFRP Laminate

*** Further loading after failure

Series **R90°** – Specimen 1: Test Results

Load (kN)	Vertical Slip between Flange and Web(mm)*		Horizontal Separation between Flange and Web(mm)*		Remarks
	Left side(#1)	Right side(#2)	Left side(#3)	Right side(#4)	
0	0.00	0.00	0.00	0.00	
21	0.63	0.24	0.00	0.00	
40	0.83	0.37	0.00	0.00	
60	1.00	0.50	0.00	0.01	
81	1.17	0.64	0.07	0.05	
93	1.53	0.84	0.04	0.08	Ultimate Load **
68	5.13	1.64	0.09	0.08	Web slipping *** (Left side & Right side)
89	8.11	3.16	0.12	0.27	
72	12.45	7.07	-1.28	0.93	Testing terminated (Snapping noise of steel ties)

* Downward vertical displacements are positive and outward horizontal separations are positive

** Initiation of Partial delamination (Shear cracks) of GFRP Laminate

*** Further loading after failure

Series **R90°** – Specimen 2: Test Results

Load (kN)	Vertical Slip between Flange and Web(mm)*		Horizontal Separation between Flange and Web(mm)*		Remarks
	Left side(#1)	Right side(#2)	Left side(#3)	Right side(#4)	
0	0.00	0.00	0.00	0.00	
20	0.49	0.13	0.00	0.00	
40	0.71	0.29	0.00	0.00	
60	0.83	0.41	0.00	0.00	
81	0.97	0.51	0.04	0.00	
95	1.27	0.63	0.12	0.02	Ultimate Load **
69	3.43	0.93	-1.00	0.03	Web slipping *** (Left side)
96	9.63	2.23	-1.00	0.16	****
84	12.61	2.84	-1.00	0.19	Testing terminated (Snapping noise of steel ties)

* Downward vertical displacements are positive and outward horizontal separations are positive

** Initiation of Partial delamination (Shear cracks) of GFRP Laminate

*** Further loading after failure

**** Post-slip failure load higher than initial ultimate load

Series **R90°** – Specimen 3: Test Results

Load (kN)	Vertical Slip between Flange and Web(mm)*		Horizontal Separation between Flange and Web(mm)*		Remarks
	Left side(#1)	Right side(#2)	Left side(#3)	Right side(#4)	
0	0.00	0.00	0.00	0.00	
20	0.17	0.53	0.00	0.00	
39	0.34	0.81	0.02	0.00	
61	0.57	1.05	0.07	0.01	
78	1.10	1.34	0.23	0.03	Ultimate Load **
60	2.45	1.61	0.20	0.03	Web slipping *** (Left side & Right side)
72	5.38	2.33	-0.46	0.08	
69	14.07	12.00	-2.38	-0.23	Testing terminated (Snapping noise of steel ties)

* Downward vertical displacements are positive and outward horizontal separations are positive

** Initiation of Partial delamination (Shear cracks) of GFRP Laminate

*** Further loading after failure

Series **R90°/0°** – Specimen 1: Test Results

Load (kN)	Vertical Slip between Flange and Web(mm)*		Horizontal Separation between Flange and Web(mm)*		Remarks
	Left side(#1)	Right side(#2)	Left side(#3)	Right side(#4)	
0	0.00	0.00	0.00	0.00	
20	0.28	0.20	0.00	0.00	
40	0.44	0.37	0.00	0.00	
60	0.55	0.53	0.00	0.00	
80	0.66	0.65	0.00	0.01	
99	0.75	0.75	0.00	0.02	
122	0.93	0.88	0.00	0.04	
140	1.21	1.05	0.00	0.05	Ultimate Load **
131	1.65	1.17	0.00	0.06	
148	2.12	1.32	0.00	0.06	****
105	4.36	1.74	0.00	0.07	Web slipping *** (Left side)
141	10.18	3.12	0.00	0.18	Testing terminated (Snapping noise of steel ties)

* Downward vertical displacements are positive and outward horizontal separations are positive

** Initiation of vertical rupture of GFRP Laminate

*** Further loading after failure

**** Post-slip failure load higher than initial ultimate load. Failure of laminate: complete rupture and partial delamination of GFRP laminate

Series **R90°/0°** – Specimen 2: Test Results

Load (kN)	Vertical Slip between Flange and Web(mm)*		Horizontal Separation between Flange and Web(mm)*		Remarks
	Left side(#1)	Right side(#2)	Left side(#3)	Right side(#4)	
0	0.00	0.00	0.00	0.00	
20	0.82	0.26	0.00	0.00	
40	1.09	0.54	0.00	0.00	
60	1.25	0.70	0.00	0.00	
79	1.37	0.81	0.00	0.00	
100	1.5	0.92	0.03	0.01	
120	1.63	1.01	0.08	0.01	
132	1.92	1.10	0.17	0.01	Ultimate Load **
119	2.76	1.25	0.36	0.01	Web slipping *** (Left side)
144	8.35	2.38	0.87	0.09	****
123	14.29	8.68	1.31	0.07	Testing terminated (Snapping noise of steel ties)

* Downward vertical displacements are positive and outward horizontal separations are positive

** Initiation of vertical rupture of GFRP Laminate

*** Further loading after failure

**** Post-slip failure load higher than initial ultimate load. Failure of laminate: complete rupture and partial delamination of GFRP laminate

Series **R90°/0°** – Specimen 3: Test Results

Load (kN)	Vertical Slip between Flange and Web(mm)*		Horizontal Separation between Flange and Web(mm)*		Remarks
	Left side(#1)	Right side(#2)	Left side(#3)	Right side(#4)	
0	0.00	0.00	0.00	0.00	
20	0.19	0.00	0.00	0.00	
41	0.40	0.03	0.01	0.01	
59	0.50	0.20	0.00	0.02	
79.5	0.61	0.31	0.00	0.00	
102	0.75	0.45	0.03	0.06	
122	0.87	0.54	0.06	0.08	
136	1.78	0.81	0.37	0.09	Ultimate Load **
108	7.53	1.70	-0.18	0.10	Web slipping *** (Left side)
127	8.94	2.80	-0.74	0.16	****
113	13.65	7.71	-2.33	-1.04	Testing terminated (Snapping noise of steel ties)

* Downward vertical displacements are positive and outward horizontal separations are positive

** Initiation of vertical rupture of GFRP Laminate

*** Further loading after failure

**** Failure of laminate: complete rupture and partial delamination of GFRP laminate

Series **R(90°/0°)^2** - Specimen 1: Test Results

Load (kN)	Vertical Slip between Flange and Web(mm)*		Horizontal Separation between Flange and Web(mm)*		Remarks
	Left side(#1)	Right side(#2)	Left side(#3)	Right side(#4)	
0	0.00	0.00	0.00	0.00	
39	0.54	0.12	0.00	0.00	
80	0.81	0.40	0.02	0.00	
119	1.04	0.60	0.06	0.01	
162	1.26	0.77	0.10	0.03	
201	1.51	0.94	0.15	0.06	
233	1.9	1.16	0.23	0.11	Ultimate Load **
228	4.97	1.95	0.11	0.18	Testing terminated***

* Downward vertical displacements are positive and outward horizontal separations are positive

** Tensile splitting of concrete blocks in left flange

*** Delamination of GFRP laminates from concrete block

Series **R(90°/0°)²** - Specimen 2: Test Results

Load (kN)	Vertical Slip between Flange and Web(mm)*		Horizontal Separation between Flange and Web(mm)*		Remarks
	Left side(#1)	Right side(#2)	Left side(#3)	Right side(#4)	
0	0.00	0.00	0.00	0.00	
40	0.74	0.46	0.04	0.01	
80	1.30	0.74	0.04	0.03	
122	1.59	0.93	0.04	0.04	
162	1.86	1.09	0.09	0.06	
209	2.49	1.38	0.19	0.10	Ultimate Load
190	6.08	2.06	0.51	0.10	Web slipping (Left side)
226	9.23	3.39	0.01	0.22	Testing terminated**

* Downward vertical displacements are positive and outward horizontal separations are positive

** Post-slip failure load higher than initial ultimate load. Tensile splitting of concrete blocks in left flange followed by delamination of GFRP laminate from concrere block

Series **R(90°/0°)^2** - Specimen 3: Test Results

Load (kN)	Vertical Slip between Flange and Web(mm)*		Horizontal Separation between Flange and Web(mm)*		Remarks
	Left side(#1)	Right side(#2)	Left side(#3)	Right side(#4)	
0	0.00	0.00	0.00	0.00	
39	0.02	0.57	0.00	0.01	
79	0.25	0.97	0.00	0.02	
120	0.44	1.32	0.01	0.04	
159	0.61	1.60	0.03	0.06	
202	0.92	1.91	0.11	0.11	
228	2.87	2.79	0.40	0.19	Ultimate Load**
198	5.09	3.41	-0.56	0.22	Testing terminated***

* Downward vertical displacements are positive and outward horizontal separations are positive

** Tensile splitting of concrete blocks in left flange

*** Delamination of GFRP laminates from concrete block

Series **R45°/135°** – Specimen 1: Test Results

Load (kN)	Vertical Slip between Flange and Web(mm)*		Horizontal Separation between Flange and Web(mm)*		Remarks
	Left side(#1)	Right side(#2)	Left side(#3)	Right side(#4)	
0	0.00	0.00	0.00	0.00	
40	0.27	0.30	0.00	0.01	
80	0.50	0.57	0.01	0.02	
120	0.67	0.76	0.03	0.04	
162	0.87	0.92	0.05	0.08	
200	1.11	1.07	0.13	0.13	
214	1.32	1.17	0.23	0.15	Ultimate Load**

* Downward vertical displacements are positive and outward horizontal separations are positive

** Complete delamination of GFRP laminate from flange of intersection, followed by snapping noise of steel ties

Series **R45°/135°** – Specimen 2: Test Results

Load (kN)	Vertical Slip between Flange and Web(mm)*		Horizontal Separation between Flange and Web(mm)*		Remarks
	Left side(#1)	Right side(#2)	Left side(#3)	Right side(#4)	
0	0.00	0.00	0.00	0.00	
41	0.39	0.64	0.00	0.00	
79	0.61	0.98	0.00	0.02	
120	0.81	1.25	0.04	0.04	
158	1.00	1.49	0.07	0.08	
200	1.19	1.72	0.14	0.14	
229	1.43	1.95	0.23	0.21	Ultimate Load**

* Downward vertical displacements are positive and outward horizontal separations are positive

** Complete delamination of GFRP laminate from flange of intersection, followed by snapping noise of steel ties

Series **R45°/135°** – Specimen 3: Test Results

Load (kN)	Vertical Slip between Flange and Web(mm)*		Horizontal Separation between Flange and Web(mm)*		Remarks
	Left side(#1)	Right side(#2)	Left side(#3)	Right side(#4)	
0	0.00	0.00	0.00	0.00	
41	0.50	0.63	0.00	0.00	
81	0.99	0.95	0.00	0.07	
121	1.40	1.23	0.02	0.11	
162	1.61	1.45	0.01	0.16	
199	1.95	1.87	-0.04	0.25	Ultimate Load**

* Downward vertical displacements are positive and outward horizontal separations are positive

** Complete delamination of GFRP laminate from flange of intersection, followed by snapping noise of steel ties